

Synthesis and Characterization of Porous Metal Oxides and Core-shell Nanoparticles

A thesis submitted in partial fulfilment

for the degree of

Master of Science

as a part of the

Integrated Ph. D. programme

(Material Science)

by

Sisir Maity



Chemistry and Physics of Materials Unit

Jawaharlal Nehru Centre for Advanced Scientific Research

(A Deemed University)

Bangalore, India

March 2013

*Dedicated to My Family
and Teachers*

DECLARATION

I hereby declare that the matter embodied in the thesis entitled “*Synthesis and Characterization of Porous Metal Oxides and Core-shell Nanoparticles*” is the result of investigations carried out by me at the Chemistry and Physics of Materials Unit, Jawaharlal Nehru Centre for Advanced Scientific Research, Bangalore, India under the supervision of Prof. Eswaramoorthy Muthusamy and that it has not been submitted elsewhere for the award of any degree or diploma.

In keeping with the general practice in reporting scientific observations, due acknowledgement has been made whenever the work described is based on the findings of other investigators. Any omissions that might have occurred due to oversight or error in judgment is regretted.

Sisir Maity

CERTIFICATE

I hereby certify that the work described in this thesis “*Synthesis and Characterization of Porous Metal Oxides and Core-shell Nanoparticles*” has been carried out by Mr. Sisir Maity under my supervision at the Chemistry and Physics of Materials Unit, Jawaharlal Nehru Centre for Advanced Scientific Research, Bangalore, India and that it has not been submitted elsewhere for the award of any degree or diploma.

Prof. Eswaramoorthy Muthusamy

(Research Supervisor)

ACKNOWLEDGEMENT

I am very pleased to thank my research supervisor Prof. Eswaramoorthy Muthusamy for his constant guidance, support and encouragement. I shall always be thankful to him for giving me the academic freedom to learn beyond the obvious.

I would like to thank present and past Int. Ph. D. Co-ordinator and Chairman, Prof. S. Balasubramanian, Prof. T. K. Maji and Prof. G. U. Kulkarni for their constant help and support.

I thank the following faculties namely Prof. S. Balasubramanian, Prof. A. Sundaresen, Prof. M. Ewaramoorthy, Prof. G. U. Kulkarni, Prof. K. S. Narayan, Prof. N. Chandrabhas, Prof. T. K. Maji, Prof. A. Govindaraj, Prof. A. Chakrabarty from CPMU, JNCASR; Prof. Swapan K. Pati, Prof. Umesh V. Wagmare, Prof. S. Narasimhan from TSU, JNCASR; Prof. H. Ila, Dr. S. Rajaram, Dr. Subi J. George, Dr. T. Govindaraju, Dr. Ujjal K. Gautam, Dr. R. Biswanathan, Dr. S. Peter from NCU, JNCASR; Prof. S. M. Shivaprasad, Dr. R. Ganapathy, Dr. R. Dutta form ICMS, JNCASR for their valuable courses.

I would like to thank Mr. Somnath for helping me to do XRD measurement.

I am extremely thankful to the technical staff namely Ms. Selvi (for FESEM); Mrs. T. Usha, Dr. J. Ghatak, Dr. Karthik (for TEM); Mr. Vasu (for UV, PL, IR and TGA), Mr. Anil (for XRD); Mr. Kishore (for SEM); Mr. Sunil, Mr. Sreenath, Mr. Srinivas Rao and Mr. Srinivas (for technical assistance).

I am greatly thankful to JNCASR Library, Complab, Academics, Administration and Security who always try their best to make our life smooth at the campus.

I also thank all of my present lab mates Mr. Piyush, Mr. Pawan, Mr. Amrit, Mr. Sonu, Mr. Dheeraj, Mr. Krishna, and Ms. Soumya T. for their co-operation and company

and making a good friendly environment in the lab. I specially thank Mr. Piyush for his useful suggestions and discussions on the research problems. I thank my past lab mates Dr. Saikrishna, Dr. K. K. R. Datta, Mrs. Josena for their helpful suggestions. I also thank to all summer and POCE students for giving a good company.

I would like to thank my Int. Ph. D. batch mates Koushik, Anirban, Ram, Chandan De, Chandan Kumar, Ankush, Arkamita and Rajshekhar for their constant support and encouragement and also for making enjoyable atmosphere during course work and project.

Thanks to all my JNC friends Sudip, Partha, Arup, Gautam, Debabrata, Suman, Rana, Nitesh, Urmi, Krishnendu B, Sudeshna, Pralok, Dibyajyoti, Somananda, Arpan H, Ritesh, Syamantak, Suresh, Jayaram, Anindita, Nivedita, Arpan D, Varun, Moorthy, Srinivas, Avijit Saha, Somnath, Avijit Sen, Rajib, Tarak, Moumita, Sunita, Swastika, Wasim, Pallabi B, Rajdeep, Soumik, Chidambar, Ankit, Mohit, Bhawani, Ramana, Bharath, Jiaul, Jiarul, Saikat C, Narendra, Sumanta, Uttam, Chandradhish, Monali, Moses, Promoda, Rajkumar, Sohini, Anananya B, Shivakumar, Shatunu, Vikash and also my all school, college and IISC friends Prokriti, Ajay, Tirthaprasad with whom I really enjoyed.

I am highly grateful to my high school and undergraduate teachers to help me in understanding the basics of science and clarifying my doubts.

Finally I thank my family. Thanks to my parents who always give me support and encouragements and my brother for always being with me. Thanks to all my teachers from whom I learn a lot beyond the academic world.

Thank you all for being with me.

PREFACE

The thesis consists of three chapters. Chapter 1 gives a brief overview of nanomaterials, size dependent properties of nanomaterials and why they are different from the bulk, various aspects of synthesis procedure with controlling the shape and size and their applications.

In chapter 2, we demonstrate novel synthetic routes of porous metal oxides using template method. These porous oxides have foam-like architecture containing macropores and show appreciable BET surface area.

Chapter 3 deals with the synthesis and characterization of core-shell nanoparticles. Highly dispersed gold nanoparticles were formed on the surface of hematite spindles and titania coating was then carried out to form the core-shell structure.

Table of Content

DECLARATION.....	iii
CERTIFICATE.....	v
ACKNOWLEDGEMENT.....	vii
PREFACE.....	ix
Table of Content.....	xi

Chapter 1: Introduction to Nanomaterials

1.1 Introduction.....	15
1.2 Why Nanomaterials are Different?	17
1.2.1 Size Effects.....	17
1.2.2 Surface Effects.....	17
1.2.3 Quantum Confinement Effects.....	18
1.3 Synthesis of Nanomaterials.....	20
1.3.1 Sol-gel Method.....	20
1.3.2 Solvothermal Method.....	21
1.3.3 Chemical Precipitation.....	21
1.3.4 Pyrolysis.....	22
1.4 Applications of Nanomaterials.....	22
1.4.1 Nanoelectronics.....	23
1.4.2 Bio-applications.....	23

1.4.3 Environmental Clean-up.....	24
1.4.4 Catalysis.....	24
1.5 Conclusions.....	27
1.6 Refences.....	28

Chapter 2: Carbon Spheres Assisted Synthesis of Porous Metal Oxides

Summary.....	33
2.1 Introduction.....	34
2.2 Scope of the Present Work.....	35
2.3 Strategy for the synthesis of Popous Metal Oxides.....	35
2.4 Experimental Section.....	37
2.5 Sample Characterization.....	39
2.6 Results and Disscussion.....	39
2.6.1 Morphology.....	39
2.6.2 Powder XRD Analysis.....	42
2.6.3 N ₂ Adsorption-Desorption Isotherms.....	44
2.7 Conclusion.....	47
2.8 References.....	48

Chapter 3: Synthesis and Characterization of Core-Shell Nanoparticles

Summary.....	51
3.1 Introduction.....	52
3.2 Scope of the Present Work.....	54
3.3 Experimental Section.....	55
3.4 Sample Characterization.....	56
3.5 Results and Discussion.....	57
3.6 Conclusion.....	76
3.7 References.....	77

Chapter 1

Introduction to Nanomaterials

1.1 Introduction:

Nanomaterials are the materials having at least one of its dimensions in nanometer ($1 \text{ nm} = 10^{-9} \text{ m}$) range. Figure 1 gives a general idea of objects correlating to different sizes.^[1]

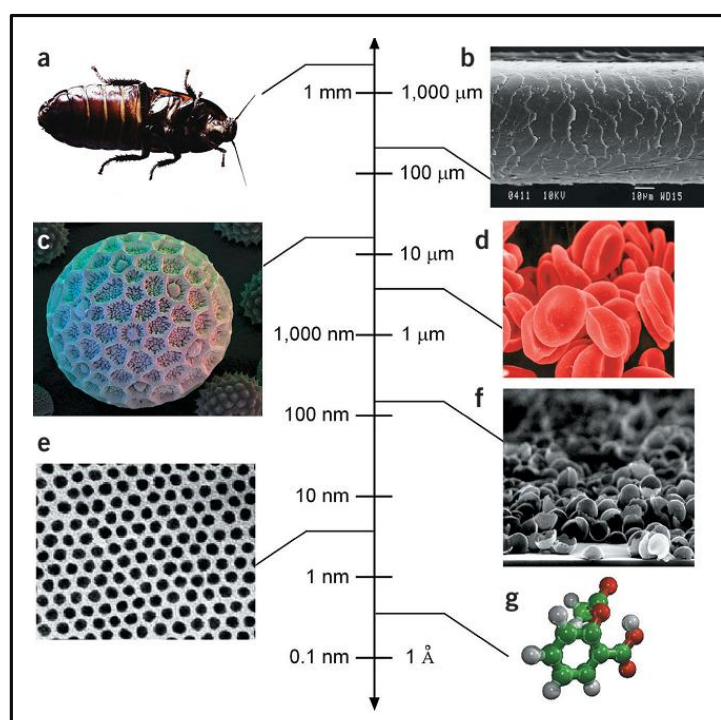


Figure 1: Sizes of representative ‘small’ objects with different length scales (a) A cockroach, (b) A human hair (c) Polygonum pollen grain, (d) Red blood cells, (e) Cobalt nanocrystal superlattice, (f) An aggregate of half-shells of palladium and (g) Aspirin molecule (Ref. 1-reprinted with permission).

Nanomaterials are classified based on their dimensionalities as (3–n) dimensional where n is the number of dimensions in nano-regime. According to that nanomaterials are

zero-dimensional (0D, nanocrystals), one-dimensional (1D, nanowires and nanotubes) and two-dimensional (2D, nanofilms). Table-1 lists the typical nanomaterials of different dimensions.^[2]

Table 1: Examples of nanomaterials of different dimensionalities:

	Size (approx.)	Materials
(a) 0D-Nanocrystals and clusters (quantum dots)	1–10 nm	Metals, semiconductors, magnetic materials
Other Nanoparticles	1–100 nm	Ceramic oxides
(b) 1D-Nanowires	1–100 nm	Metals, semiconductors, oxides, sulfides, nitrides
Nanotubes	1–100 nm	Carbon, layered metal chalcogenides
(c) 2D- arrays of nano particles	some nm ² –mm ²	Metals, semiconductors, magnetic materials
Surfaces and thin films	thickness 1–1000 nm	Various materials
(d)3D-Structures (superlattices)	some nm in all three dimensions	Metals, semiconductors, magnetic materials

Various studies on physical and chemical properties of nanomaterials have been carried out over the past three decades and are recently become one of the most interesting research areas in chemistry, solid state physics, biology, medicine, electronics, engineering etc. due to their unique size and shape dependent properties. Special characteristic properties like, high surface to volume ratio and quantum confinement make them physically and chemically different from their bulk. Nanomaterials for their size dependent properties find enormous applications in catalysis,^[3-6] drug delivery,^[7, 8]

photo electronics,^[9-11] memory storage devices,^[12, 13] energy storage,^[14] optical display,^[15] sensor and detectors,^[16] bio-medical application^[17, 18] etc.

1.2 Why Nanomaterials are Different?

1.2.1 Size Effects:

Gold in the bulk form is known as a shiny, yellow noble metal having a face centred cubic structure, is non-magnetic and its melting point is 1063 °C. However, at nano-regime, its optical property is totally different from the bulk gold. For example, 10 nm gold particles absorb green light and thus appear red. The melting temperature decreases dramatically as the size goes down.^[19] Bulk gold is known to be noble, but 2–3 nm nanoparticles exhibit excellent catalytic property.

1.2.2 Surface Effects:

Surface atoms have lesser number of neighbours than atoms in the bulk. The smaller particle, the larger fraction of atoms at the surface compared to volume. The surface-to-volume ratio increases with decreasing in size and therefore there exist a numerous properties like melting point, other phase transition temperature etc which are completely different from their bulk.^[20-23] Edge and corner atoms have a lower coordination and bind foreign atoms or molecules more tightly and therefore, small clusters behave like molecules than as bulk and showing completely different properties.^[21]

The fraction of atoms at the surface with respect to its volume called dispersion F , varies with surface to volume ratio (shown in the equation below). The size dependence of dispersion for cubes of n atoms along an edge and a total of $N=n^3$ atoms is shown in Figure-2.^[24]

$$F = \frac{6n^2 - 12n + 8}{n^3} = \frac{6}{N^{1/3}} \left(1 - \frac{2}{N^{1/3}} + \frac{8}{6N^{2/3}}\right) \approx \frac{6}{N^{1/3}}$$

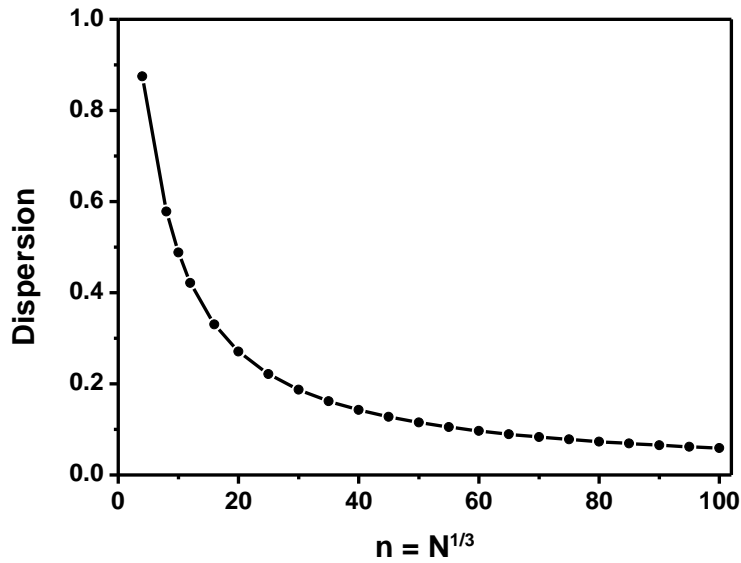


Figure-2: Evolution of the dispersion F as a function of n for cubic clusters up to $n = 100$ ($N=10^6$)

1.2.3 Quantum confinement effects:

For a metal, the Fermi level is in the centre of a band and even in its smaller size, the room temperature energy (kT) may exceed the electronic energy level spacing. In semiconductors, the Fermi level lies in between two bands and the spacing remains large even at small sizes. The HOMO (highest occupied molecular orbital)-LUMO (lowest occupied molecular orbital) gap increases in semiconductor nanocrystals for smaller sizes. The size dependence is shown schematically in Figure-3.^[25]

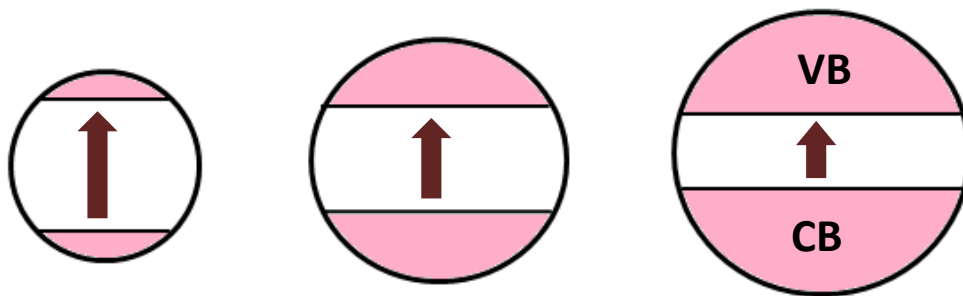


Figure-3: Schematic representation of the size effect on the gap between the valence band (VB) and the conduction band (CB). Smaller particles have a wider band gap.

The size dependence of the HOMO–LUMO band gap is best observed in the luminescence properties of semiconductor nanoparticles. It is shown in Figure-4 for the fluorescence properties of colloidal CdSe–ZnS core–shell nanoparticles.^[26] The fluorescence property can be tuned by adjusting the particle size between blue at 1.7 nm diameter and red at 6 nm.^[27]



Figure-4: Fluorescence of CdSe–ZnS core–shell nanoparticles with diameter of 2.7 nm (blue) up to 5 nm (red), giving evidence of the scaling of the semiconductor band gap with particle size (Ref. 26- reprinted with permission).

1.3 Synthesis of Nanomaterials:

In the last two decades, research has been developed extensively in the synthetic methods of new nanomaterials of different sizes and shapes. Generally nanomaterials can be synthesized either by top-down (continuous division of matter from bulk) approach or by bottom-up (controlled growth of constituents starting from atoms) approach.

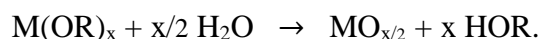
A few examples of synthetic methods normally used to produce nanostructured materials through top-down and bottom-up approaches are given below:

1.3.1 Sol-Gel Method:

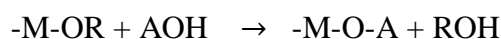
The sol-gel method is based on the inorganic polymerization of metal or non-metal alkoxide including four steps: hydrolysis, polycondensation, drying and thermal decomposition.^[28] The metal or non-metal alkoxides first hydrolyze in presence of water or alcohols according to the hydrolysis process



If m is equal to x, the reaction is totally hydrolysed, followed by the condensation of water or alcohol and thus



In addition of an acid or a base to the reaction mixture, can also help to hydrolyze the precursor. In the case of an acid, the reaction takes place between alkoxide and the acid.



The solvent must be removed after condensation of the solution. Higher temperature calcination is necessary to decompose the organic precursor. The size of the sol particles depends on the solution composition, pH and temperature. By controlling these factors, one can tune the size of the particles. Using this method several metal oxide nanostructures such as TiO_2 ,^[29-33] ZrO_2 ,^[34] CeO_2 ,^[35] ZnO ,^[36] SnO_2 ^[37] could be synthesized.

1.3.2 Solvothermal Method:

In this method, precursor's solution is heated at higher temperature than the boiling point of the solvent inside a sealed autoclave. The vapour pressure at higher temperature of the solvent than its boiling point is much higher due to high autogenous pressures which act the important role to transform the precursor materials to its nanostructure. Products obtained in this procedure are generally crystalline compared to other solution based reactions. During the synthesis of nanocrystals, parameters such as solvent vapour-pressure, temperature, reaction time can be varied to get different size and shape. Various types of nanomaterials such as Fe_2O_3 ,^[38-40] Fe_3O_4 ,^[41] TiO_2 ,^[42] ZrO_2 ,^[43] BaTiO_3 ,^[44] SrTiO_3 ,^[45] Sb_2S_3 .^[46]

1.3.3 Chemical Precipitation:

The nucleation and growth of nanometer-sized materials involves the process of chemical precipitation to a solid phase from a homogeneous solution. The control over the precipitation helps to improve the growth of nanoparticles to the desired size and shape leading to monodispersed nanoparticles. By controlling the factors like pH, concentration of the precursors and ions, temperature etc, different types of nanoparticles

with narrow size distributions, such as $\text{Zr}(\text{OH})_4$,^[47] BaTiO_3 ,^[48] CdTe ^[49] etc. have been synthesized.

1.3.4 Pyrolysis:

Pyrolysis involves the decomposition of different chemical species or their mixtures at appropriate temperature to get a solid compound and unwanted products evaporate away. In this process, products formed are powders having a wide size distribution in the micrometer range. For some cases, the reaction rate of decomposition needs to be slow to get uniform distribution of nanomaterial. Generally, MCO_3 , MC_2O_4 , $\text{M}(\text{C}_2\text{O}_2)$, $\text{M}(\text{CO})_x$, MNO_3 , glycolate, citrate, alkoxides etc. are the common precursors used. Poly vinyl alcohol (PVA) and poly ethylene glycol (PEG) are commonly used as protecting agents. Different kinds of nanoparticles including metals, metal oxides, semiconductors and composite materials such as Ag ,^[50] Au ,^[51] Ni ,^[52] TiO_2 ,^[53] ZrO_2 ,^[54] Al_2O_3 ,^[55] SnO_2 ,^[55] GaN ^[56] etc have been prepared using this method.

Apart from the above procedures there are various procedures for the synthesis of nanomaterials like micelles as template, ball milling, self assembly, chemical vapour deposition (CVD), physical vapour deposition (PVD), different lithographic techniques, molecular beam epitaxy (MBE) etc.

1.4 Applications of Nanomaterials:

The successful and explosive development of nanomaterials distinctly leads to their various applications in industrial, technical, bio-medical and environmental purposes. Few of applications are given below:

1.4.1 Nanoelectronics:

Metal clusters behaving as quantum dots are becoming the fundamental materials in nanoelectronics and nanotechnology. This is simply due to their ability to enable single electron storage and tunnelling^[57-60] and also studied that ligand stabilized very small (1-2 nm) gold clusters can be charged by a single electron which is then stored in the particle.^[61, 62] Thus these kinds of particles behave ultimately as very small transistors working at room temperature. Modern microtransistors are lithographically generated on silicon surfaces. They are large enough to be mechanically contacted (~200 nm) and their arrangement on the silicon wafer is performed by the lithographic process. Many efforts have been initiated to solve the various problems and to make these more promising.

1.4.2 Bio-applications:

Remarkable efforts have been made in the evolution of the magnetic nanoparticles (MNPs) and improvement for their bio-applications. Suitable shape and surface functionalization of MNPs is vital for their physicochemical properties, colloidal stability and biological behaviour. For pharmaceutical and biomedical purposes, magnetic nanoparticles should have very small and narrow size distribution with high magnetization values. MNPs with tailored surface properties have been broadly studied for various applications such as drug delivery, hyperthermia, magnetic resonance imaging (MRI), tissue engineering and repair, biosensing, biochemical separations and bio-analysis.^[18]

1.4.3 Environmental Clean-up:





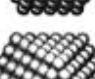
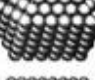
Nanomaterials have a great potential for the efficient removal of pollutants and biological contaminants from the environment. Porous nanomaterials of high surface area with different morphologies and functionalized with suitable ligands are widely used as adsorbents and catalysts for the detection and removal of gases^[63, 64] (SO₂, CO, NO_x etc.), contaminated chemicals^[65] (arsenic, chromium, manganese, nitrate, mercury, lead, bismuth and other metal ions etc.), organic pollutants^[66] (aliphatic and aromatic hydrocarbons) and biological substances, such as viruses, bacteria, parasites and antibiotics etc.^[67] The novel nanoscaled materials are developed for the treatment of drinking water contaminated by toxic metal ions, radionuclides, organic and inorganic materials, industrial wastages, bacteria, viruses etc and the treatment of air. The environmental applications of nanocomposites in photocatalytic degradation, the adsorption of pollutants and pollutant sensing and detection result in a greener environment.

1.4.4 Catalysis:

The use of metal nanoparticles in heterogeneous catalysis is well established. The number of surface atoms increases with decrease in particle size compared to its bulk and thus small metal particles behave as highly reactive catalyst as surface atoms are the active centres for catalytic process. Among the surface atoms, those sitting on the edges and corners are more active than those in planes due to their low co-ordination number. The percentage of edge and corner atoms also increases with decrease in size (Table-2) and this is why very small metal particles are preferred as catalysts.^[68] So the catalytic

properties of some single phase materials can be improved by preparing them as nanostructures.

Table 2: The relation between the total number of atoms in full shell clusters and the percentage of surface atoms (Ref. 68- reprinted with permission):

Full-shell Clusters	Total Number of Atoms	Surface Atoms (%)
1 Shell 	13	92
2 Shells 	55	76
3 Shells 	147	63
4 Shells 	309	52
5 Shells 	561	45
7 Shells 	1415	35

Because of the increased activity, there are significant cost advantages in fabricating catalysts from nanomaterials. Catalysts based on the activity of metal nanoparticles can only be heterogeneous type. For industrial processes the metal nanoparticles are generated on supports such as alumina, silica, charcoal or other oxide based materials by impregnating these substrates with solution of the corresponding metal salt. Appropriate reduction processes make the salts into zero-valent nanoparticles. Such procedures produce particles of various sizes. Since the large particles are less active than

smaller ones, only a portion of metal particles actually contribute to the catalytic process. Routes to uniform nanoparticles synthesis are therefore a research goal.

For example, gold known as noble and inert in bulk shows high catalytic activity in nanometre level supported with oxide materials. Such catalytic effects have been reported for CO oxidation where the maximum activity seen with gold nanoparticles of ~2-3 nm in diameter.^[69-71] The oxidation of ethylene glycol was found to be optimum on carbon supported gold nanoparticles of ~7 nm in diameter.^[72] The catalytic activity of gold nanoparticles for the reduction of p-nitrophenol decreases after 8 nm in size.^[73] A great number of organic reactions are reported over the few years catalysed by gold nanoparticles.^[74, 75] Several metal nanoparticles like Pt, Pd, Ag, Ni, Cu, Rh, Ru etc. supported with oxide nanoparticles like Fe₂O₃, Fe₃O₄, TiO₂, ZnO, CuO, NiO, CeO₂, ZrO₂, Al₂O₃, SiO₂^[76, 77] etc. have been studied in details for their catalytic activity in various oxidation-reduction reactions and also in photo catalytic reactions.

Mesoporous metal oxides generated a great deal of interest for their potential application as catalysts as well as catalytic supports for hydrogenation, alkylation and various oxidation-reduction reactions. This is because the structure of mesoporous materials can achieve an optimum compromise of high site density and good transport characteristics.^[6]

Organic-inorganic hybrid nanomaterials have also shown good catalytic activity in multi-step chemical process in a one-pot reactor (cascade reaction) due to their different structural arrangements and hierarchical pores. The combination of different precursors of organic and inorganic moieties during preparation of hybrid materials allows them unique properties for efficient catalytic activity and as supports.

1.5. Conclusions:

Research in the field of nanoscience for the last two decades has been greatly progressed only in terms of synthesis, fundamental understandings and applications. Elemental composition, shapes and control over sizes of nanostructures have been studied continuously from time to time using various methods. Over the last decade, nanomaterials are successfully applied to various catalysis, sorption, electronics and biological system. Though there are significant improvements in certain synthetic procedures to obtain nanomaterials with some specific size and functions, still lot more to be done to obtain variety of nanomaterials of different shapes and dimensions.

1.6. References:

- [1] G. Whitesides, *Nat. Biotechnol.* **2003**, *21*, 1161.
- [2] C. N. R. Rao, A. K. Cheetham, *J. Mater. Chem.* **2001**, *11*, 2887.
- [3] V. Polshettiwar, R. Luque, A. Fihri, H. Zhu, M. Bouhrara, J.-M. Basset, *Chem. Rev.* **2011**, *111*, 3036.
- [4] D. Urbano, B. Daniel, C. Avelino, *Chem. Soc. Rev.* **2013**.
- [5] L. Xiaobo, Y. Yan, Y. Qihua, *J. Mater. Chem. A* **2013**, *1*, 1525.
- [6] B. Viswanathan, B. Jacob, *Catalysis Reviews* **2005**, *47*, 1.
- [7] M. Vallet-Regí, F. Balas, D. Arcos, *Angew. Chem. Int. Ed.* **2007**, *46*, 7548.
- [8] E. Climent, R. Martínez-Máñez, F. Sancenón, M. Marcos, J. Soto, A. Maquieira, P. Amorós, *Angew. Chem. Int. Ed.* **2010**, *49*, 7281.
- [9] S. Karg, W. Riess, M. Meier, M. Schworer, *Synth. Met.* **1993**, *57*, 4186.
- [10] L. Brus, *J. Phys. Chem.* **1986**, *90*, 2555.
- [11] M. W. Alam, Z. Wang, S. Naka, H. Okada, *Appl. Phys. Lett.* **2013**, *102*, 061105.
- [12] B. G. Levi, *Phys. Today* **2004**, *57*, 24.
- [13] J. L. Simonds, *Phys. Today* **1995**, *48*, 26.
- [14] P. V. Kamat, *J. Phys. Chem. C* **2007**, *111*, 2834.
- [15] M. Aspelmeyer, P. Meystre, K. Schwab, *Phys. Today* **2012**, *65*, 29.
- [16] A. Mandelis, *Phys. Today* **2012**, *65*, 60.
- [17] M. Vallet-Regí, *Journal of internal medicine* **2010**, *267*, 22.
- [18] L. H. Reddy, J. L. Arias, J. Nicolas, P. Couvreur, *Chem. Rev.* **2012**, *112*, 5818.
- [19] M. Schmidt, R. Kusche, B. Von Issendorff, H. Haberland, *Nature* **1998**, *393*, 238.

- [20] G. Breaux, R. Benirschke, T. Sugai, B. Kinnear, M. Jarrold, *Phys. Rev. Lett.* **2003**, *91*, 215508.
- [21] K. M. Unruh, T. E. Huber, C. A. Huber, *Phys. Rev. B* **1993**, *48*, 9021.
- [22] S. L. Lai, J. Y. Guo, V. Petrova, G. Ramanath, L. H. Allen, *Phys. Rev. Lett.* **1996**, *77*, 99.
- [23] K. Koga, T. Ikeshoji, K.-i. Sugawara, *Phys. Rev. Lett.* **2004**, *92*, 115507.
- [24] E. Roduner, Nanoscopic Materials: Size-Dependent Phenomena, *The Royal Society of Chemistry, Cambridge* **2006**.
- [25] E. Roduner, *Chem. Soc. Rev.* **2006**, *35*, 583.
- [26] I. L. Medintz, H. T. Uyeda, E. R. Goldman, H. Mattoussi, *Nat Mater* **2005**, *4*, 435.
- [27] A. Eychmüller, *J. Phys. Chem. B* **2000**, *104*, 6514.
- [28] C. Burda, X. Chen, R. Narayanan, M. El-Sayed, *Chem. Rev.* **2005**, *105*, 1025.
- [29] Y. Li, T. White, S. H. Lim, *Rev. Adv. Mater. Sci* **2003**, *5*, 211.
- [30] G. Colón, M. C. Hidalgo, J. A. Navío, *Catal. Today* **2002**, *76*, 91.
- [31] N. Uekawa, J. Kajiwara, K. Kakegawa, Y. Sasaki, *J. Colloid Interface Sci.* **2002**, *250*, 285.
- [32] A. J. Maira, K. L. Yeung, J. Soria, J. M. Coronado, C. Belver, C. Y. Lee, V. Augugliaro, *Appl. Catal. B* **2001**, *29*, 327.
- [33] H. Parala, A. Devi, R. Bhakta, R. A. Fischer, *J. Mater. Chem.* **2002**, *12*, 1625.
- [34] J. L. Woodhead, *Sci. Ceram.* **1983**, *12*, 179.
- [35] A. Chatterjee, D. Chakravorty, *J. Mater. Sci.* **1992**, *27*, 4115.
- [36] D. Mondelaers, G. Vanhoyland, H. Van den Rul, J. D'Haen, M. K. Van Bael, J. Mullens, L. C. Van Poucke, *Mater. Res. Bull.* **2002**, *37*, 901.

- [37] A. Jitianu, Y. Altindag, M. Zaharescu, M. Wark, *J. Sol-Gel Sci. Technol.* **2003**, 26, 483.
- [38] W. Wu, X. Xiao, S. Zhang, J. Zhou, L. Fan, F. Ren, C. Jiang, *J. Phys. Chem. C* **2010**, 114, 16092.
- [39] C.-J. Jia, L.-D. Sun, F. Luo, X.-D. Han, L. J. Heyderman, Z.-G. Yan, C.-H. Yan, K. Zheng, Z. Zhang, M. Takano, *J. Am. Chem. Soc.* **2008**, 130, 16968.
- [40] C.-J. Jia, L.-D. Sun, Z.-G. Yan, L.-P. You, F. Luo, X.-D. Han, Y.-C. Pang, Z. Zhang, C.-H. Yan, *Angew. Chem. Int. Ed.* **2005**, 44, 4328.
- [41] W.-F. Ma, Y. Zhang, L.-L. Li, L.-J. You, P. Zhang, Y.-T. Zhang, J.-M. Li, M. Yu, J. Guo, H.-J. Lu, C.-C. Wang, *ACS Nano* **2012**, 6, 3179.
- [42] J. Yang, S. Mei, J. M. F. Ferreira, *Mater. Sci. Eng. C* **2001**, 15, 183.
- [43] A. A. Burukhin, B. R. Churagulov, N. N. Oleynikov, *High Press. Res.* **2001**, 20, 255.
- [44] S. Wei Lu, B. I. Lee, Z. Lin Wang, W. D. Samuels, *J. Cryst. Growth* **2000**, 219, 269.
- [45] C. Chen, X. Jiao, D. Chen, Y. Zhao, *Mater. Res. Bull.* **2001**, 36, 2119.
- [46] S. H. Yu, L. Shu, Y. S. Wu, Y. T. Qian, Y. Xie, L. Yang, *Mater. Res. Bull.* **1998**, 33, 1207.
- [47] H. Yue-xiang, G. Cun-ji, *Powder Technol.* **1992**, 72, 101.
- [48] H. S. Potdar, S. B. Deshpande, S. K. Date, *Mater. Chem. Phys.* **1999**, 58, 121.
- [49] M. Gao, S. Kirstein, H. Möhwald, A. L. Rogach, A. Kornowski, A. Eychmüller, H. Weller, *J. Phys. Chem. B* **1998**, 102, 8360.
- [50] W. Cai, L. Zhang, *J. Phys.: Condens. Matter* **1997**, 9, 7257.

- [51] L. Maya, M. Paranthaman, T. Thundat, M. L. Bauer, *J. Vac. Sci. Technol. B* **1996**, *14*, 15.
- [52] A. Valentini, N. Carreño, amp, x, L.V, L. F. D. Probst, E. R. Leite, E. Longo, *Microporous Mesoporous Mater.* **2004**, *68*, 151.
- [53] L. E. Depero, P. Bonzi, M. Musci, C. Casale, *J. Solid State Chem.* **1994**, *111*, 247.
- [54] W. Li, L. Gao, J. K. Guo, *Nanostruct. Mater.* **1998**, *10*, 1043.
- [55] D. Lindackers, C. Janzen, B. Rellinghaus, E. F. Wassermann, P. Roth, *Nanostruct. Mater.* **1998**, *10*, 1247.
- [56] Y. Yang, V. J. Leppert, S. H. Risbud, B. Twamley, P. P. Power, H. W. H. Lee, *Appl. Phys. Lett.* **1999**, *74*, 2262.
- [57] K. Ilgweon, H. Sangyeon, H. Kwangseok, L. Jongho, S. Hyungcheol, *IEEE Electron Device Letters* **1999**, *20*, 630.
- [58] L. I. Glazman, *J. Low Temp. Phys.* **2000**, *118*, 247.
- [59] D. V. Averin, K. K. Likharev, *J. Low Temp. Phys.* **1986**, *62*, 345.
- [60] A. Kongkanand, P. V. Kamat, *ACS Nano* **2007**, *1*, 13.
- [61] G. Schön, U. Simon, *Colloid. Polym. Sci.* **1995**, *273*, 101.
- [62] G. Schön, U. Simon, *Colloid. Polym. Sci.* **1995**, *273*, 202.
- [63] J. A. Rodriguez, *Prog. Surf. Sci.* **2006**, *81*, 141.
- [64] R. M. Heck, R. J. Farrauto, S. T. Gulati, Catalytic Air Pollution Control, Third Edition, *John Wiley & Sons, Inc.* **2009**.
- [65] N. Wu, H. Wei, L. Zhang, *Environ. Sci. Technol.* **2011**, *46*, 419.
- [66] N. Savage, M. Diallo, *J. Nanopart. Res.* **2005**, *7*, 331.
- [67] M. M. Khin, A. S. Nair, V. J. Babu, R. Murugan, S. Ramakrishna, *Energy & Environmental Science* **2012**, *5*, 8075.

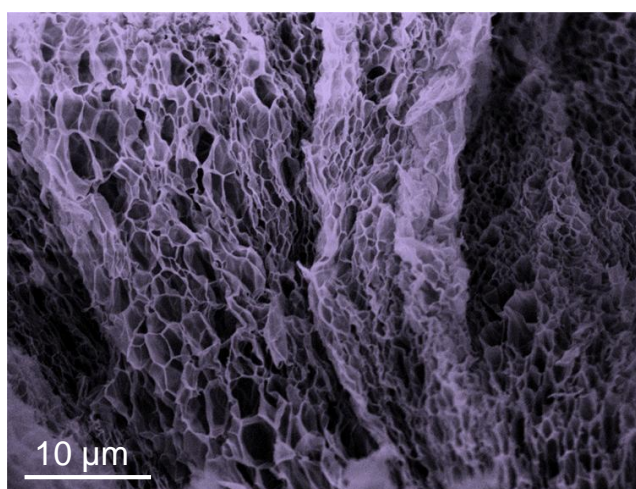
- [68] K. J. Klabunde, *Nanoscale Materials in Chemistry*, Wiley-Interscience **2001**.
- [69] L. Guzzi, G. Petö, A. Beck, K. Frey, O. Geszti, G. Molnár, C. Daróczy, *J. Am. Chem. Soc.* **2003**, *125*, 4332.
- [70] S. H. Overbury, V. Schwartz, D. R. Mullins, W. Yan, S. Dai, *J. Catal.* **2006**, *241*, 56.
- [71] M. Valden, X. Lai, D. W. Goodman, *Science* **1998**, *281*, 1647.
- [72] S. Biella, F. Porta, L. Prati, M. Rossi, *Catal. Lett.* **2003**, *90*, 23.
- [73] S. Panigrahi, S. Basu, S. Praharaj, S. Pande, S. Jana, A. Pal, S. K. Ghosh, T. Pal, *J. Phys. Chem. C* **2007**, *111*, 4596.
- [74] A. S. K. Hashmi, G. J. Hutchings, *Angew. Chem. Int. Ed.* **2006**, *45*, 7896.
- [75] A. S. K. Hashmi, *Chem. Rev.* **2007**, *107*, 3180.
- [76] J. Shi, *Chem. Rev.* **2012**, *113*, 2139.
- [77] D. Zhang, G. Li, J. C. Yu, *J. Mater. Chem.* **2010**, *20*, 4529.

Chapter 2

Carbon Spheres Assisted Synthesis of Porous Metal Oxides

Summary*

In this chapter, a facile route for the synthesis of foam-like porous oxides using carbon spheres and polyvinylpyrrolidone (PVP) as sacrificial templates is discussed. The as-prepared porous structures were characterized by XRD, FESEM, TEM and BET methods. The porous oxides have foam like architecture and contain macropores. These foam-like macroporous oxides are formed through the fusion of oxide nanoparticles around the gas bubbles liberated during the combustion of composites and show significant BET surface areas.



* Published in J. Nanosci. Nanotechnol., 2012.

2.1 Introduction:

Synthesis of porous metal oxides is drawing a great attention due to a wide range of potential applications that have found a great utility in catalysis, sorption, fuel cell electrode materials, biofiltration and hydrogen and energy storage.^[1] The basic reason behind their diverse utility is their large internal surface area i.e. the presence of voids of controllable dimensions at nanometer and micrometer levels. Due to their functional and structural features, numerous efforts have been devoted to the synthesis, characterization and applications of porous materials over the last decade.^[2-4] Progress has been made in structural, compositional, and morphological control and the stability of porous materials by using several synthetic routes, especially templating method of synthesis.^[5] Remarkable growth has been achieved in the field of ordered porous materials with uniform channel dimensions that can be tuned over a variety of length scales.^[6] Foam-like porous materials containing multiple-sized pores would benefit from superior properties compared with single-pore sized materials due to increased mass transport across the material.^[7]

Surfactants and amphiphilic block copolymers are commonly used as templates to synthesize ordered mesoporous materials.^[2, 5] Likewise, periodic three-dimensional arrays of macropores are fabricated using latex spheres as templates.^[8] Inorganic materials with a varied pore structure could be synthesized by the combination of surfactants or amphiphilic block copolymers with macrotemplates such as colloidal crystals, polymer foams, emulsions etc.^[9] In general, formation of foam-like macroporous oxides were reported using templates such as synthetic polymer gel,^[10] cellulose acetate membrane,^[11] starch gel,^[12] agarose,^[13] egg shell membrane,^[14] wood shell structure,^[15] bacterial threads.^[16] Recently, self-supporting porous frameworks of metals and metal oxides were

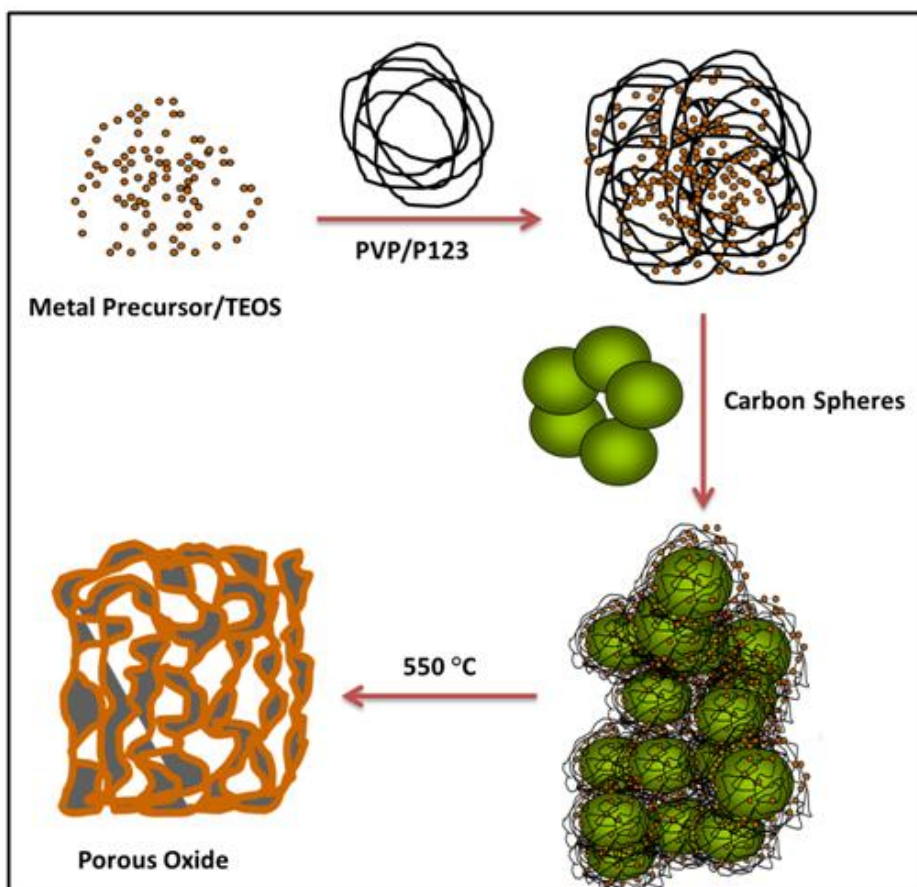
prepared by heating metal salts containing pastes of polysaccharide, dextran to high temperatures.^[17] This method involves heating of dextran-metal salt composite pastes at 500-900 °C which gives inorganic monoliths with sponge like structure. A similar combustion route using surfactants like triton X-100 to form porous silver monolith was also reported in the literature.^[18] Of late, template free method has also been exploited to make porous metal nanostructures.^[19]

2.2 Scope of the Present Work:

Nanostructured porous materials are very interesting research topic in past two decades for their high specific surface area. The impact of these materials are very important from the academic as well as industrial point of view due to their different pore sizes (from nanometer to millimeter), order or irregular arrangement of pores and various chemical compositions. These materials have a great prospective in heterogeneous catalysis involved in various environmental applications. For improved activity, the multifunctionality in catalytic processes should be revisited in terms of their fabrication and design from appropriate building blocks. In this chapter, we demonstrate a facile route for synthesis of foam-like porous oxides using carbon spheres and polyvinylpyrrolidone (PVP) as sacrificial templates.

2.3 Strategy for the Synthesis of Porous Oxides:

The method adopted for synthesis of porous oxides with foam-like architecture is shown in the Scheme 1. Carbon spheres are primarily made up of carbonized glucose with carboxylic and olefin functionalities.^[20] These were used as porogens as well as the adsorption centers for the metal precursors as they have negatively charged functional surface resulting from the -COOH and -OH groups.



Scheme 1: Illustration showing the formation of foam-like porous oxides.

PVP is used to bring the carbon spheres in close proximity which will facilitate the fusion of nanoparticles formed over the carbon spheres (during calcination) to form interconnected network structure. Combustion of the metal nitrate precursors loaded carbon-PVP composite in air at 550 °C generates enormous amount gases creating the void structures. The comparatively slow and extended decomposition of carbon spheres with respect to the nitrates helps to stabilize the metal oxide nanoparticles nucleated from the precursors. Further fusion of these nanoparticles around the gas bubbles leads to self-supported nanostructured walls around the large cavities. The formation of foam structure is dependent on both carbon spheres and PVP polymer. If carbon spheres were used without PVP, the calcined products results in the formation of individual metal oxide

hollow spheres.^[21, 22] If PVP was used without carbon spheres then it resulted in formation of porous networks without any foam structure.

2.4 Experimental Section:

2.4.1 Synthetic procedure for carbon spheres:

Carbon spheres of size in the range of 400 to 500 nm were prepared by hydrothermal method.^[20] In a typical procedure, 5 g of glucose dissolved in 50 mL of water to form a clear solution. The solution was placed in a 60 mL Teflon-lined sealed stainless steel container and heated at 180 °C for 12 h. The solid brown product was isolated and purified by repeated washing with ethanol and then dried at 80 °C for 4 h. The as-prepared carbon spheres along with PVP were used as templates to synthesize the porous metal oxides.

2.4.2 Synthetic procedure for porous metal oxides:

In a typical synthesis, 0.5 g of MNO_3 (where M = Ni, Cr and Cu) was dissolved in 20 mL of 1:1 water and ethanol mixture. To this solution, 1 g polyvinylpyrrolidone (Aldrich, $M_w=13,00,000$) polymer and 50 mg of carbon spheres (prepared separately) were added and mixed thoroughly to make a homogeneous viscous slurry. The slurry was then poured into a glass petri dish (50 mm diameter) and aged for 10 h in an oven at 80 °C. The transparent film of MNO_3 -PVP composite thus obtained was calcined at 550 °C for duration of 5 h with a heating rate of 1 °C min^{-1} . The sample was cooled to room temperature at a rate of 3 °C min^{-1} .

2.4.3 Synthetic procedure for porous PZT (Lead zirconate titanate):

Molar compositions of the starting materials was fixed as $\text{Pb}(\text{NO}_3)_2 : \text{Zr}(\text{OC}_3\text{H}_7)_4 : \text{Ti}(\text{OC}_3\text{H}_7)_4 : \text{PVP} : \text{CH}_3\text{COCH}_2\text{COCH}_3 : \text{H}_2\text{O} : \text{CH}_3\text{OC}_2\text{H}_4\text{OH} : n\text{-C}_3\text{H}_7\text{OH} = 1.1 : 0.53 : 0.47 : 1 : 0.5 : 2 : 30 : 0.98$, where the mole ratio for the PVP is defined for the monomer. Briefly, 3.64 g of $\text{Pb}(\text{NO}_3)_2$ was dissolved in 24 mL of methoxyethanol. To this solution 2.22 g of polyvinylpyrrolidone (Aldrich, $M_w=13,00,000$) was added. Upon addition, the solution became viscous. To this, 0.51 mL of acetylacetonate, 2.37 mL of 70% zirconium *n*-propoxide in *n*-propanol, and 1.40 mL titanium iso-propoxide were added successively. When the solution became transparent, 50 mg of carbon spheres were added. The resultant slurry was heated at 70 °C for 2 h with constant stirring. Upon cooling to room temperature, 0.4 mL of water was added and kept at room temperature for 40 h. The mixture was centrifuged and the residue rich in carbon was transferred into a petri dish, made into a thin film and dried at 80 °C. The dried composite film was calcined at 700 °C for 5 h with a heating rate of 1 °C min⁻¹. The sample was cooled to room temperature at a rate of 3 °C min⁻¹ to yield yellow colored flaky PZT material.

2.4.4 Synthetic procedure for porous SiO₂:

To 1.8 g of pluronic P123, 0.45 g of octane and 0.26 g of tri-methyl benzene (TMB) were added followed by addition of 2.57 g of tetraethylorthosilicate (TEOS). This mixture was stirred over a water bath at 50 °C for 2 minutes so as to obtain a well homogenized sol-gel mixture. 1 mL of an acidified aqueous solution (0.1 M hydrochloric acid) was added to the mixture so as to form a quaternary system (P123/hydrocarbons/TEOS/H₂O-HCl). In the microemulsion system, the molar ratio of P123 to octane was kept at 2:0.5 and that of P123 to TMB was kept at 2:0.25. On addition

of the acidified aqueous solution, the sol-gel mixture turned into a viscous gel. On leaving this gel at ambient conditions for 10 minutes resulted in a clear liquid. Now 50 mg of carbon spheres was added to this solution. The viscous brown slurry obtained was kept in an oven at 45 °C for 12 h so to ensure the evaporation of all the solvent. The resulting monolithic fragments were calcined at 550 °C for 5 h to ensure the removal of the surfactant and the carbon spheres.

2.5 Sample characterization:

The morphologies of the samples obtained in all the experiments were examined with field emission scanning electron microscope (FESEM, FEI Nova-Nano SEM-600, The Netherlands), scanning electron microscope (SEM, LeicaS-440-I Instrument, U.K), and transmission electron microscope (TEM, JEOL JEM-3010 with an accelerating voltage at 300 kV). Powder X-ray diffraction (XRD) patterns were recorded by using Bruker-D8 diffractometer using Cu K α radiation, ($\lambda=1.54 \text{ \AA}$, step size: 0.02, current: 30 mA and voltage: 40 kV). N₂ adsorption-desorption isotherms were measured with a QUANTACHROME AUTOSORB-1C surface-area analyzer at liquid nitrogen temperature (77 K).

2.6 Results and Discussion:

2.6.1 Morphology:

Figure 1a shows FESEM image of foam-like porous NiO with interconnected macroporous network extended over a large area. Higher magnification image (Figure 1b) shows the interconnected voids of size in the range of 2 to 3 μm and the wall thickness about 500 nm.

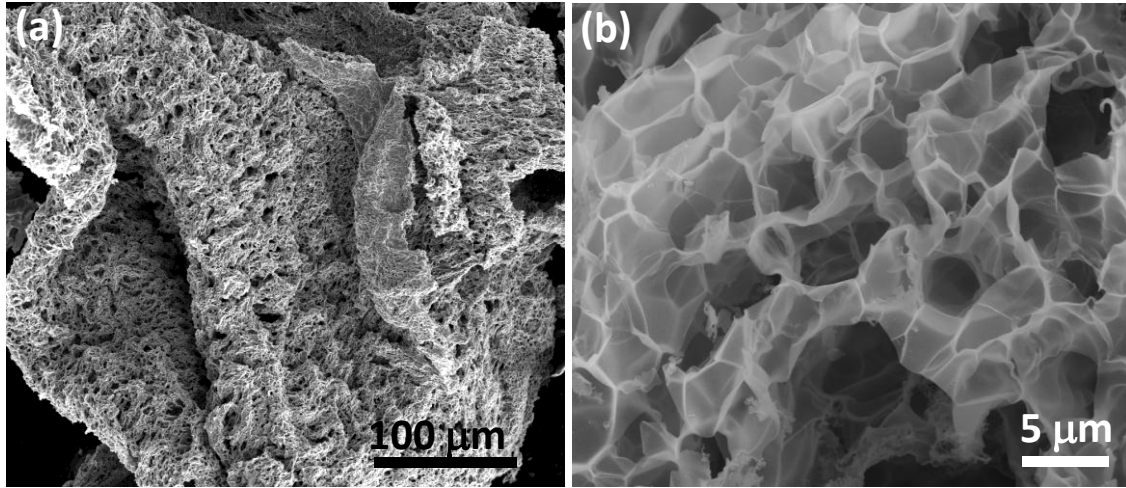


Figure 1: (a) Low-magnification FESEM image of foam-like porous networks of NiO. (b) High-magnification FESEM image of NiO.

The transmission electron microscope image of NiO (Figure 2) shows that the particle sizes are in the range of 50 to 100 nm and are fused together with the pore size between the particles about few tens of nanometer. The inset in Figure 2 shows the electron diffraction (ED) pattern of the particles that are polycrystalline in nature.

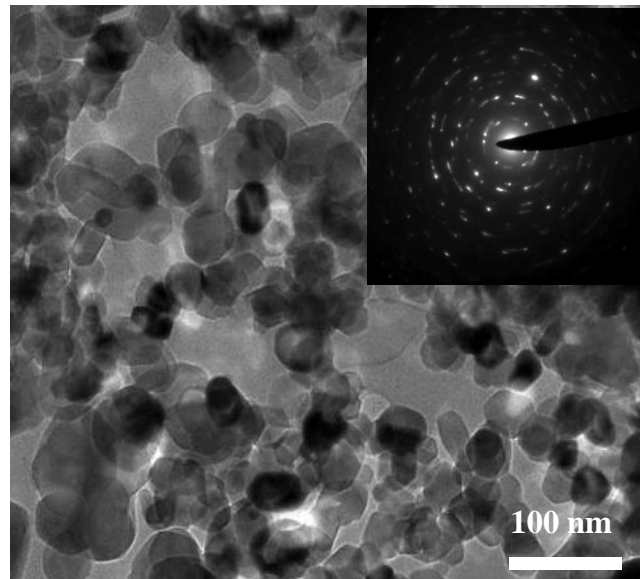


Figure 2: TEM image of NiO. Inset shows the ED pattern of NiO indicating polycrystalline nature.

Similarly, Cr_2O_3 and CuO prepared by the same method also exhibit foam-like structures (Figure 3).

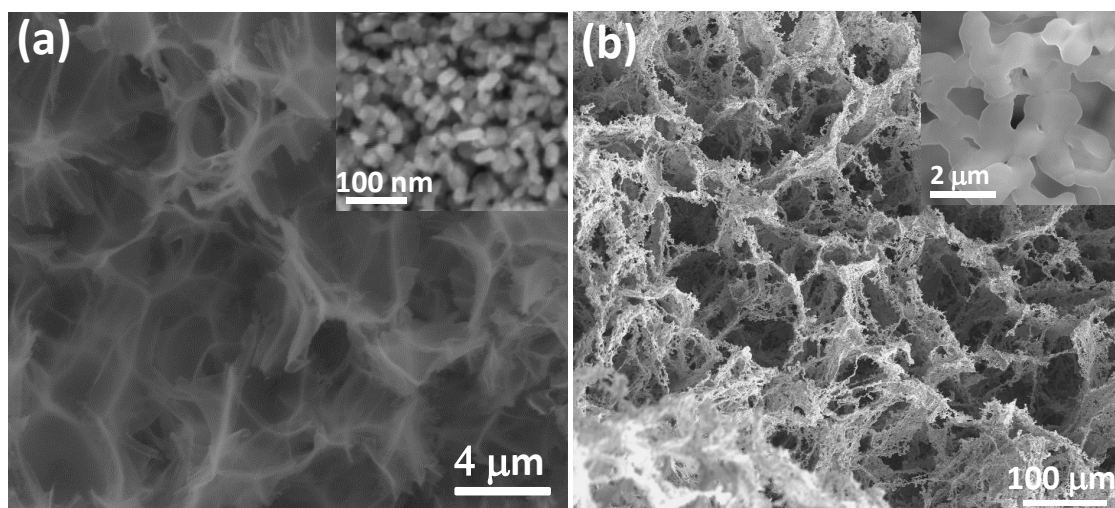


Figure 3: Low-magnification FESEM image of foam-like networks of (a) Cr_2O_3 and (b) CuO . Inset shows high-magnification image of the same.

Figure 4a shows the SEM image of the ternary oxide, PZT, after calcination which mimics the cellular structure of wood. The macropores are in the range of 1- 2 μm and the

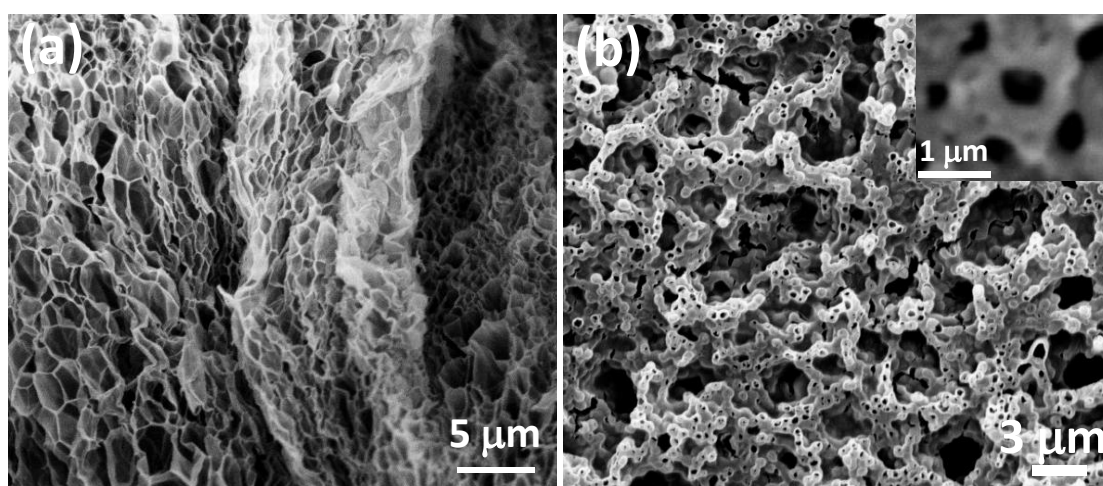


Figure 4: SEM images of (a) PZT and (b) porous SiO_2 (Inset shows the higher magnification image of the same).

wall thickness is around 0.5 - 1 μm . In the case of SiO_2 , the macropores are embedded in the network structure (Figure 4b), like hollow beads with opening around 500 nm in size.

This is in contrast to the large cavities obtained for other metal oxides whose sizes were well-beyond the size of the carbon spheres used. In the case of metal oxides, exothermic decomposition of metal nitrate precursors into nitrogen dioxide and oxygen coupled with the combustion of carbon spheres and PVP leaves large interconnected cavities of few microns in size. The absence of nanoparticulate structure with foam-like morphology when the nitrate precursors alone were heated signifies the role of carbon spheres in stabilizing the structure.

2.6.2 Powder XRD Analysis:

The powder XRD pattern of NiO (Figure 5) clearly shows peaks associated with NiO confirming the formation of crystalline NiO. Furthermore, the peak broadening suggests the existence of NiO in the form of nanoparticles.

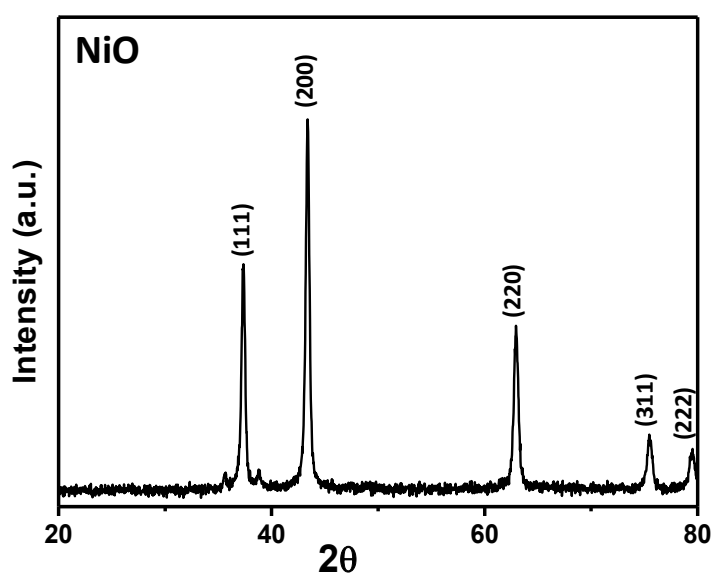


Figure 5: Powder X-ray diffraction pattern of NiO.

Figure 6-8 show the XRD pattern obtained for the porous metal oxides which are crystalline in nature with the peak broadening associated with the smaller particle size.

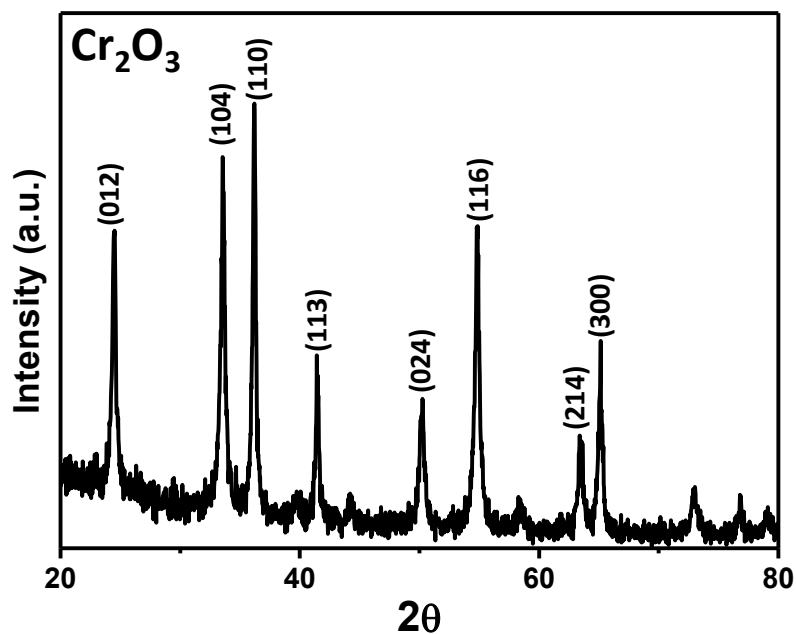


Figure 6: Powder X-ray diffraction pattern of Cr_2O_3 .

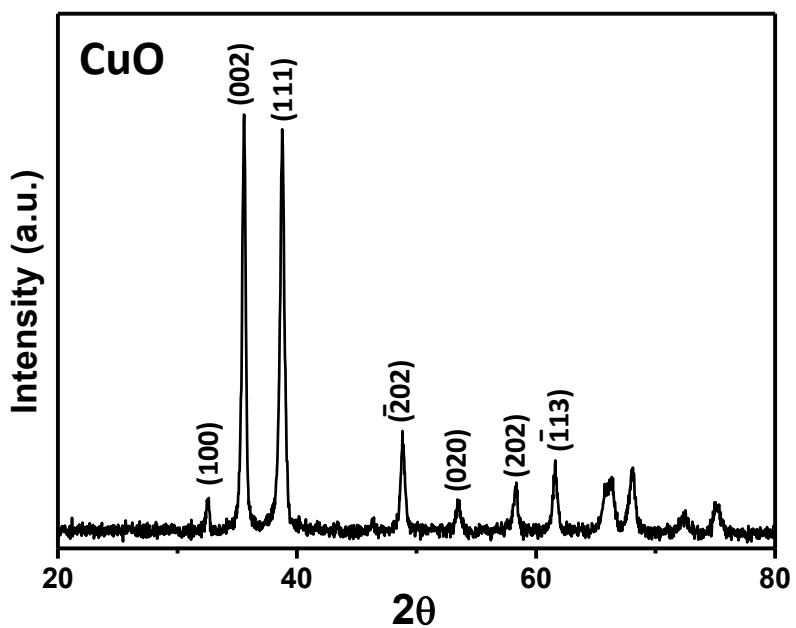


Figure 7: Powder X-ray diffraction pattern of CuO .

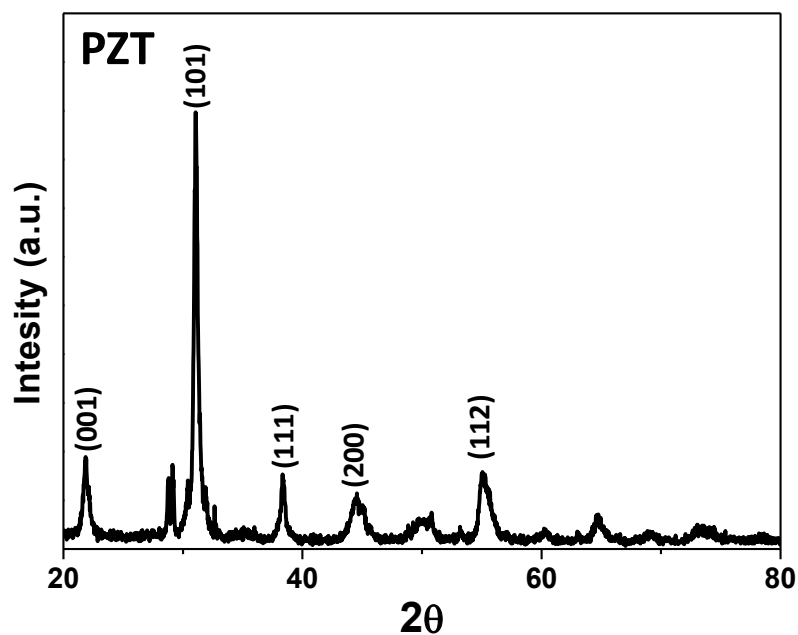


Figure 8: Powder X-ray diffraction pattern of PZT.

2.6.3 N₂ Adsorption-Desorption Isotherms:

The N₂ adsorption-desorption isotherms show Type II isotherm for all the metal oxides with no significant hysteresis (Figure 9-12). The steep uptake of nitrogen at very low P/P₀ for SiO₂ (Figure 13) suggests the presence of micropores in addition to macropores. The surface area calculated from Bruner-Emmet-Teller (BET) method are 38, 69, 67, 51 and 247 m²/g for NiO, Cr₂O₃, CuO, PZT and SiO₂ respectively.

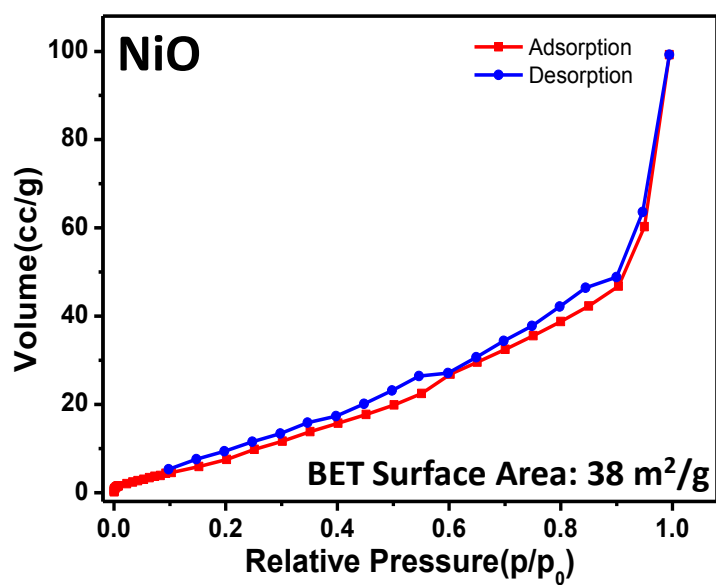


Figure 9: N₂ adsorption-desorption isotherm (at 77 K) of NiO.

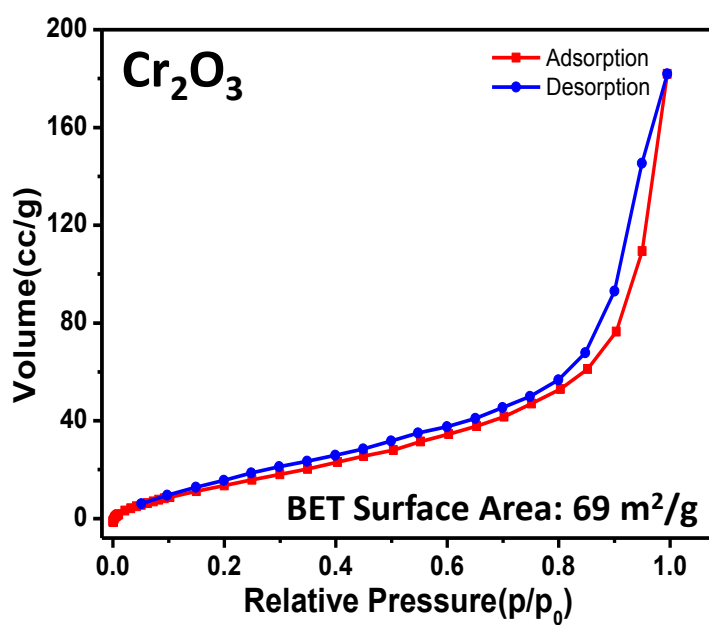


Figure 10: N₂ adsorption-desorption isotherm (at 77 K) of Cr₂O₃.

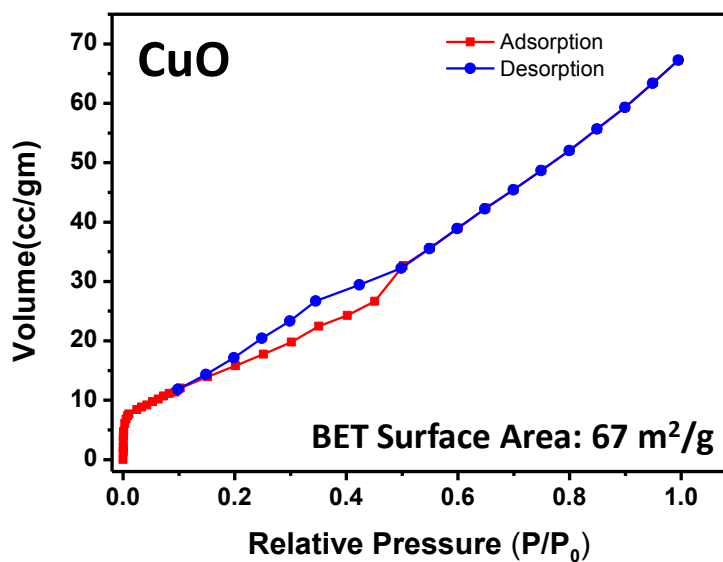


Figure 11: N_2 adsorption-desorption isotherm (at 77 K) of CuO.

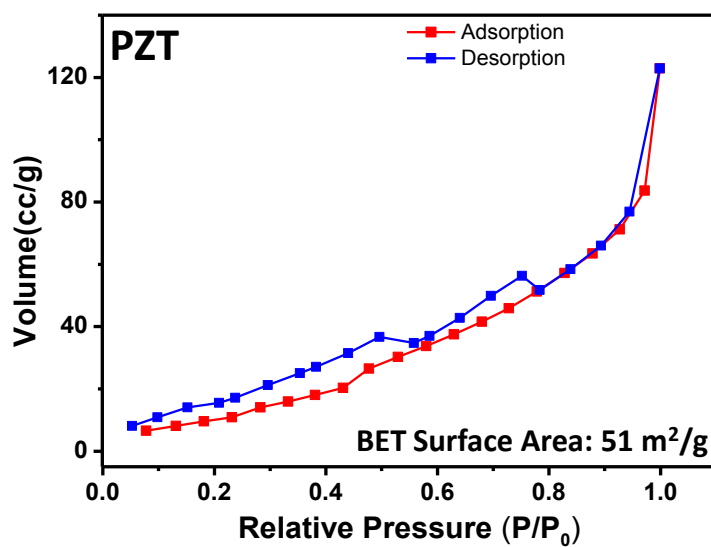


Figure 12: N_2 adsorption-desorption isotherm (at 77 K) of PZT.

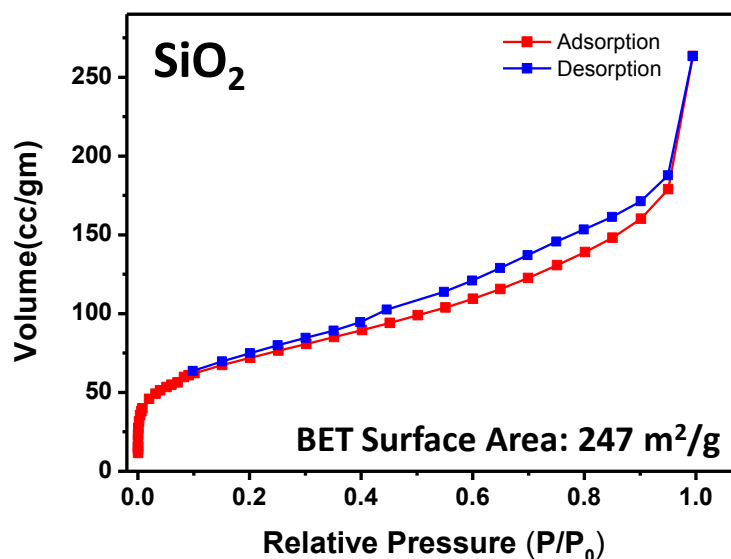


Figure 13: N₂ adsorption-desorption isotherm (at 77 K) of SiO₂.

2.7 Conclusion:

A new simple carbon spheres assisted synthetic route to form foam-like porous oxides was developed. XRD, FESEM, TEM and N₂ adsorption were carried out to characterize the porous structure. A combination of carbon spheres and PVP polymer were used as porogen with different metal precursors to achieve the foam-like architecture. The as-prepared porous oxides also have high BET surface areas. These metal oxide foam like structures could find potential applications in the fields of catalysis [23-25] and adsorbents.

2.8 References:

- [1] D. Rolison, *Science* **2003**, 299, 1698.
- [2] G. Q. Lu, X. S. Zhao, *Nanoporous Materials: Science and Engineering*, Imperial College Press **2004**, Vol. 4.
- [3] K. Ariga, M. Li, G. J. Richards, J. P. Hill, *J. Nanosci. Nanotechnol.* **2011**, 11, 1.
- [4] K. Ariga, A. Vinu, Y. Yamauchi, Q. Ji, J. P. Hill, *Bull. Chem. Soc. Jpn.* **2012**, 85, 1.
- [5] D. Zhao, J. Feng, Q. Huo, N. Melosh, G. H. Fredrickson, B. F. Chmelka, G. D. Stucky, *Science* **1998**, 279, 548.
- [6] M. Davis, *Nature* **2002**, 417, 813.
- [7] Y. Xiao-Yu, L. Yu, L. Arnaud, Y. Jia-Guo, S. Bao-Lian, *Pure Appl. Chem.* **2009**, 81, 2265.
- [8] B. T. Holland, C. F. Blanford, A. Stein, *Science* **1998**, 281, 538.
- [9] P. Yang, T. Deng, D. Zhao, P. Feng, D. Pine, B. F. Chmelka, G. M. Whitesides, G. D. Stucky, *Science* **1998**, 282, 2244.
- [10] M. Breulmann, S. A. Davis, S. Mann, H. P. Hentze, M. Antonietti, *Adv. Mater.* **2000**, 12, 502.
- [11] R. A. Caruso, J. H. Schattka, *Adv. Mater.* **2000**, 12, 1921.
- [12] B. Zhang, S. A. Davis, S. Mann, *Chem. Mater.* **2002**, 14, 1369.
- [13] J. Zhou, M. Zhou, R. Caruso, *Langmuir* **2006**, 22, 3332.
- [14] D. Yang, L. Qi, J. Ma, *Adv. Mater.* **2002**, 14, 1543.
- [15] A. Dong, Y. Wang, Y. Tang, N. Ren, Y. Zhang, Y. Yue, Z. Gao, *Adv. Mater.* **2002**, 14, 926.

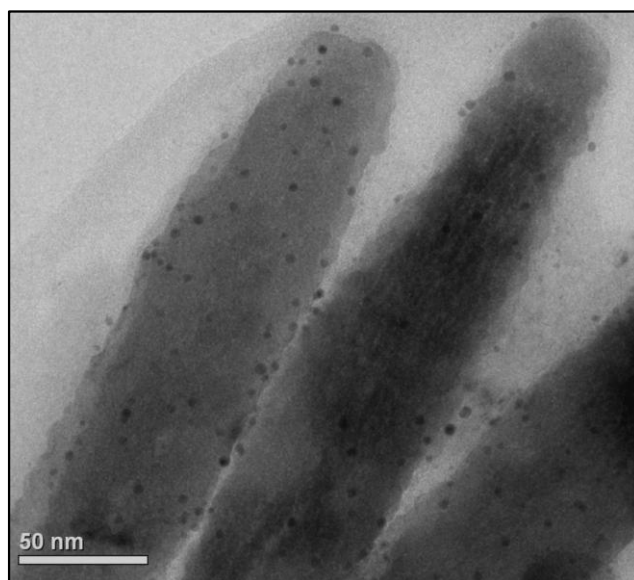
- [16] S. A. Davis, S. L. Burkett, N. H. Mendelson, S. Mann, *Nature* **1997**, 385, 420.
- [17] D. Walsh, L. Arcelli, T. Ikoma, J. Tanaka, S. Mann, *Nature Mater.* **2003**, 2, 386.
- [18] F. Khan, M. Eswaramoorthy, C. N. R. Rao, *Solid State Sciences* **2007**, 9, 27.
- [19] K. S. Krishna, C. S. S. Sandeep, R. Philip, M. Eswaramoorthy, *ACS Nano* **2010**, 4, 2681.
- [20] X. Sun, Y. Li, *Angew. Chem. Int. Ed.* **2004**, 43, 597.
- [21] X. Sun, Y. Li, *Angew. Chem. Int. Ed.* **2004**, 43, 3827.
- [22] X. Sun, J. Liu, Y. Li, *Chem. Eur. J.* **2006**, 12, 2039.
- [23] H. Thakuria, B. M. Borah, G. Das, *J. Mol. Catal. A: Chem.* **2007**, 274, 1.
- [24] Z.-R. Tian, W. Tong, J.-Y. Wang, N.-G. Duan, V. V. Krishnan, S. L. Suib, *Science* **1997**, 276, 926.
- [25] A. K. Sinha, K. Suzuki, *Angew. Chem. Int. Ed.* **2005**, 44, 271.

Chapter 3

Synthesis and Characterization of Core-Shell Nanoparticles

Summary*

In this chapter, the synthesis procedures of highly dispersed gold nanoparticles on the surface of hematite ($\alpha\text{-Fe}_2\text{O}_3$) spindles and coating of titania (TiO_2) are discussed. Also in this engineered material, a new interface having $\alpha\text{-Fe}_2\text{O}_3$, TiO_2 and gold nanoparticles altogether has been created as interfaces are the active sites for catalytic oxidation of CO.



* Work in Progress

3.1 Introduction:

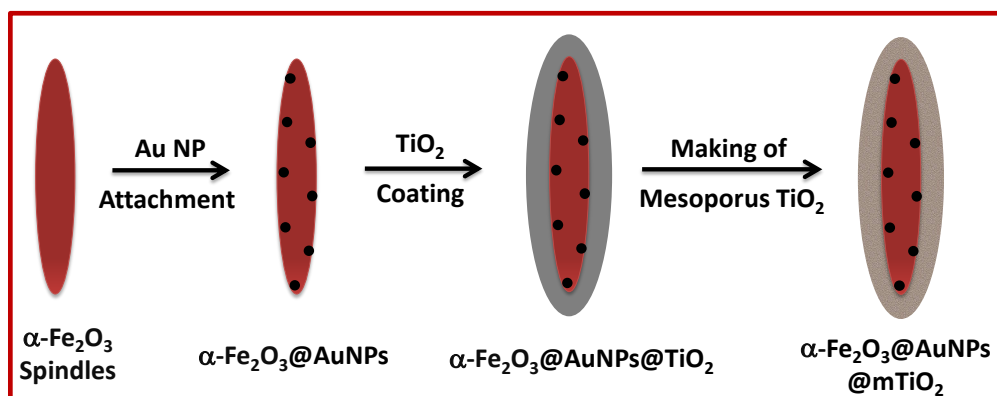
Oxidation of CO to CO₂ is a very important problem from the environmental and industrial points of view. Spontaneous emission of CO from various industrial processes or from vehicles (burning of petroleum), could cause many environmental hazards.^[1] Even at low concentration, CO can create many health problems like headache, dizziness, weakness, nausea, vomiting, vertigo, confusions, and many heart diseases.^[2] Longer exposure to CO can lead to significant damage to central nervous system and even to death.^[3] CO is troublesome for many industrial process as well, for example, presence of a trace amount of CO in different types of fuel cells makes serious problems in the distribution and storage of hydrogen feed gas.^[4, 5] It is much more necessary to purify the hydrogen feed gas in the fuel cell by reducing the CO concentration below 100 ppm.^[1, 6, 7] At different levels, CO oxidation to CO₂, is to be carried out at different temperatures. For example, low temperature oxidation of CO is most useful for air purification in long time duration of space travel and in CO₂ lasers, while a long lifetime at high temperature would be required to convert CO to CO₂ in automobile gas exhaust.^[8]

After a great discovery of catalytic property of gold in nanometer level, oxide supported gold nanoparticles have been attracted enormous interest for their high activity in large number of oxidation and reduction reactions.^[1, 9-14] Many experiment and theoretical studies have been carried out to understand the catalytic property of supported nanoparticles towards the CO oxidation.^[9-11, 14-18] Remarkably, gold nanoparticles (AuNPs) over various supports were considered as a highly active catalyst for the selective oxidation of hydrocarbons, methanol synthesis from CO₂, water-gas shift reaction, reduction of nitric oxide by hydrogen, propylene epoxidation and CO oxidation.^[19, 20] Among these reactions, the oxidation of CO to CO₂ is one of the most

studied reactions over supported gold catalyst.^[6, 21] A large number of metal oxides such as α -Fe₂O₃,^[1, 4, 22-28] TiO₂,^[8, 29-33] Co₃O₄,^[27, 34] NiO,^[27] CeO₂,^[35-39] CuO,^[40] ZnO,^[40, 41] ZrO₂,^[42-44] Al₂O₃,^[45, 46] SiO₂^[47, 48] have been used as supports for gold nanoparticles for CO oxidation. The interface between the gold nanoparticles and oxide layers plays key role during catalysis by providing the active sites for oxidation reaction where the oxygen molecules are preferentially adsorbed on the support oxide.^[49] So, the catalytic activity of gold nanoparticles strongly depends upon the nature of the supported oxides.^[10, 50] As an example, gold supported on the insulating or covalently bonded metal oxides like Al₂O₃, SiO₂ are less active than gold on α -Fe₂O₃, TiO₂, Co₃O₄, NiO etc.^[50] Detailed studied of the oxidation reaction over a temperature range indicates that Au/ α -Fe₂O₃,^[25] Au/CeO₂,^[51] Au/ZrO₂^[42] show high activity at temperatures as high as 350 °C, whereas Au/TiO₂,^[29] Au/Co₃O₄,^[10] Au/NiO^[10] are highly efficient at temperatures as low as -90 °C. The temperature dependent activity for CO oxidation on different supports arises mainly due to the ease of adsorption of CO and the ease of desorption of CO₂ at the Au-support interface.^[10] In the case of Au/TiO₂, amount of CO uptake is more at lower temperature whereas Au/ α -Fe₂O₃ can adsorb CO at higher temperature. The desorption of CO₂ is higher for Au/ α -Fe₂O₃ at high temperature and for Au/TiO₂ at low temperature. Also, in this catalysis process, one of the major concerns is the growth of the metal nanoparticles on the surface of the supports due to sintering (coalescence of particles) or Ostwald Ripening (transport of monoatomic or molecular species between individual particles).^[52] This particle size growth decreases the activity of the catalyst as well as its recyclability.^[53] Thus, there remains the need for a single high performance and stable catalyst, which could operate over the entire temperature range needed.

3.2 Scope of the Present Work:

In the present study, we have tried to overcome these challenging problems using a novel engineered catalyst design by sandwiching the active gold nanoparticles catalyst between two active supports (viz. α -Fe₂O₃ and TiO₂). As, gold nanoparticles supported over α -Fe₂O₃ are active up to 350 °C and titania supported gold nanoparticles are active at temperatures as low as -90 °C, we hypothesize by integrating these three components together we could create a catalyst which will work over -90 °C to 350 °C. As shown in the Scheme 1, at first gold nanoparticles are synthesized on the surface of α -Fe₂O₃ spindles and then a shell of titania (TiO₂) was coated onto it. Finally, the outer titania layer was made mesoporous so that, CO and O₂ molecules could reach the active sites and CO₂ could come out easily.



Scheme 1: Schematic for synthesis of core shell α -Fe₂O₃@AuNPs@mTiO₂ catalysts.

Since in our design, the gold nanoparticles are sandwiched between two oxide layers, it will not be able to grow in size due to sintering or Ostwald ripening. This will infer the catalyst stability as well high recyclability. Also in this engineered catalyst we create a new interface having α -Fe₂O₃, TiO₂ and gold nanoparticles altogether. As

interfaces are the active sites in these catalysts, this new interface might give rise to new interesting results.

3.3 Experimental Section:

3.3.1 Synthesis of α -Fe₂O₃ Spindles:

The hematite (α -Fe₂O₃) nano spindles were prepared by hydrothermal treatment of a mixture of FeCl₃ and NH₄H₂PO₄ solutions reported in the literature.^[54] In a typical experimental procedure, 3.20 mL of aqueous FeCl₃ solution (0.5 M) and 2.88 mL of aqueous NH₄H₂PO₄ solution (0.02 M) were mixed with vigorous stirring. The mixture was diluted to a final volume of 80 mL by the addition of distilled water. The solution mixture was stirred for 10 minutes and transferred to a Teflon-lined stainless-steel autoclave with a capacity of 100 mL and kept at 220 °C for hydrothermal treatment for 2 h. The autoclave was then cooled down to room temperature naturally. The precipitate was separated by centrifugation at 6000 rpm, washed with distilled water for three times and absolute ethanol and finally dried at 80 °C for overnight.

3.3.2 Synthesis of α -Fe₂O₃@AuNPs:

Gold nanoparticles (diameter ~2.5 nm) were attached on α -Fe₂O₃ surface by deposition precipitation method.^[29] In the synthesis method, 8 mL of HAuCl₄ solution of different concentrations (2, 5 and 10 mM) were prepared in aqueous medium. The pH of the solution was raised to 9 by drop wise addition of 0.1 M aqueous NaOH solution. Then 20 mg of α -Fe₂O₃ synthesized before was added with stirring at room temperature. The resulting suspension was stirred for 2 h and the pH of the solution was maintained constant at 9 by regular addition of same concentrated NaOH solution. The reaction

mixture was heated at 70 °C for 1 h with vigorous stirring. The mixture was then cooled to room temperature, centrifuged at 6000 rpm and washed with distilled water for two times. Finally the precipitate was dried at 80 °C for overnight.

3.3.3 Synthesis of α -Fe₂O₃@AuNPs@TiO₂ Material:

TiO₂ coating was carried out in ethanol-acetonitrile (3:1) solvent mixture and in ethanol at an ambient condition by hydrolyzing of tetrabutoxide orthotitanate (TBOT) in presence of ammonia following the reported procedure in the literature.^[55, 56] In the experimental procedure, 20 mg of as prepared spindle shaped particles were dispersed in 60 mL of solvent by sonication for 10 minutes. A concentrated ammonia solution (30 wt %) was added to above dispersion and stirred for 10 min. Then TBOT was added drop wise to the above mixture with stirring at 400 rpm. For ethanol-acetonitrile solvent mixture, TBOT was added at room temperature and the reaction mixture was stirred for 1.5 h. When only ethanol was used as solvent, TBOT was added at 45 °C temperature and the reaction was continued for 12 h with stirring. The resultant products were centrifuged at 3000 rpm for 5 min and washed with and ethanol for 3 times and dried at 80 °C for overnight.

3.4 Sample Characterization:

The morphologies of the samples obtained in all the experiments were characterized with field emission scanning electron microscope (FESEM, FEI Nova-Nano SEM-600, the Netherlands). Powder x-ray diffraction (PXRD) patterns were recorded using Bruker-D8 diffractometer using Cu K α radiation, ($\lambda=1.54$ Å, step size: 0.02, current: 30 mA and voltage: 40 kV). The transmission electron microscope (TEM)

images were taken on a JEOL, JEM 3010 operated at 300 kV. Samples were prepared by placing a drop of dispersion on a TEM grid (holey carbon). Electronic absorption spectra were recorded on a Perkin Elmer Lambda 900 UV-Vis-NIR Spectrometer. One cm path length cuvette was used for recording the spectra. The zeta potential measurements were carried out using a NanoZS (Malvern UK) employing a 532 nm laser at a back scattering angle of 173°.

3.5 Results and Discussion:

Hematite (α -Fe₂O₃) spindles were prepared by hydrothermal treatment of FeCl₃ solution as reported by Jia et al.^[54] The field emission scanning electron microscope (FESEM) image (Figure 1) confirms the formation of spindle shape of α -Fe₂O₃ which are

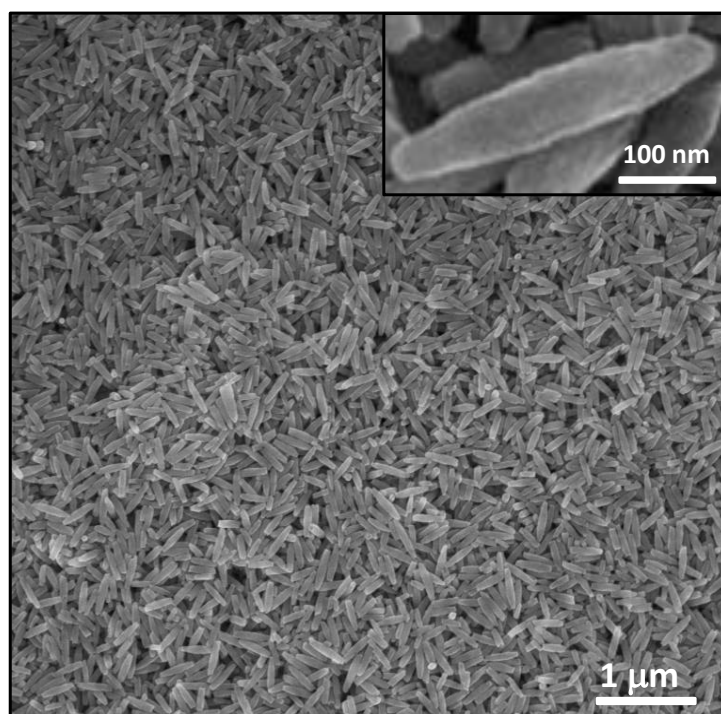


Figure 1: FESEM images of spindle shaped α -Fe₂O₃. Inset shows high magnification image of the same.

uniformly distributed in terms of their shape and size. The average length of the spindles obtained is around 370 ± 30 nm (inset of Figure 1). The powder XRD pattern (Figure 2) of spindles shows the formation of rhombohedral α - Fe_2O_3 with $R\bar{3}c$ space group. The little broadening in the peaks arises due to the small size of the spindles. The surface charge of the as synthesized spindles was measured at different pH (Figure 3). The surface of spindles became increasingly negative with rising pH.

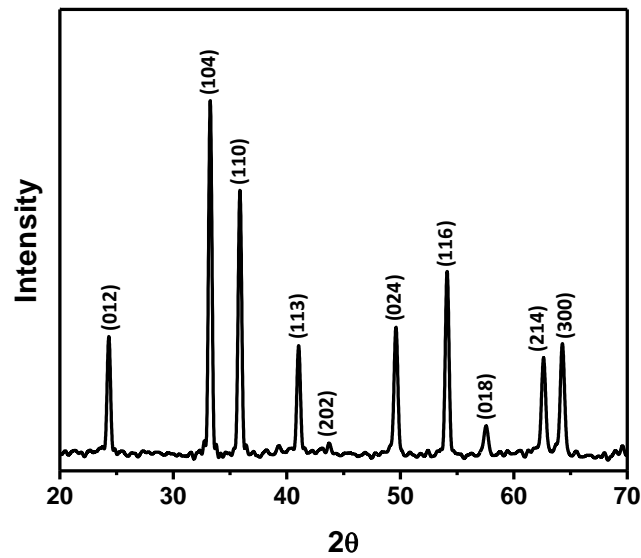


Figure 2: Powder XRD pattern of α - Fe_2O_3 .

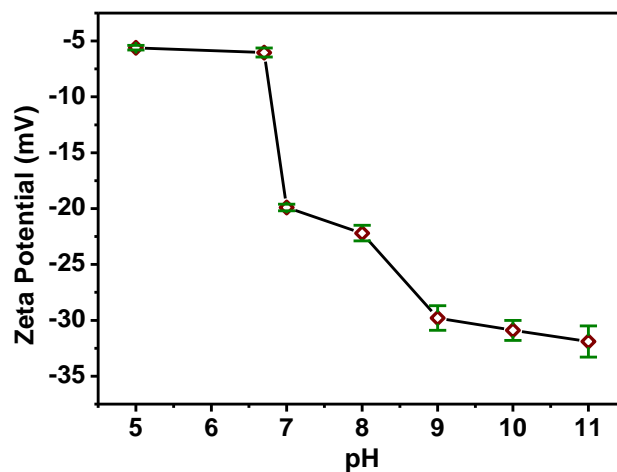
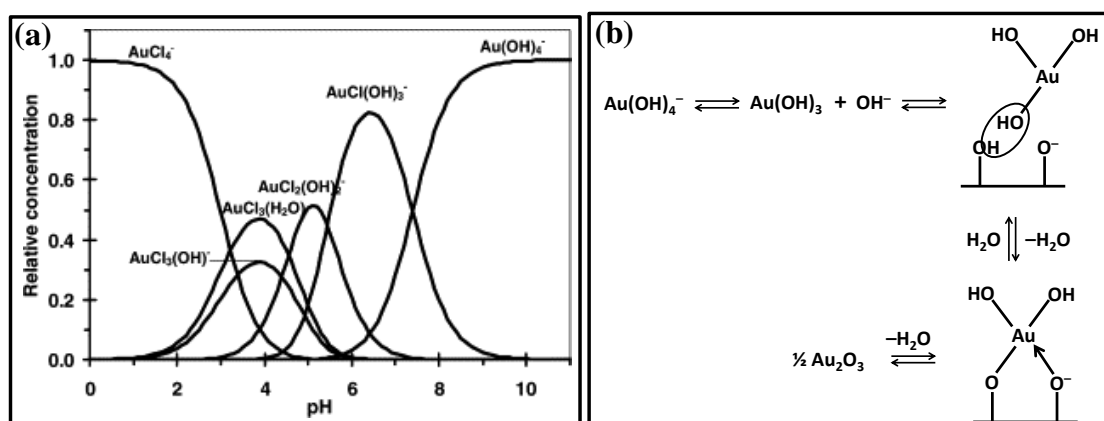


Figure 3: Zeta potential of α - Fe_2O_3 at different pH.

Gold nanoparticles were formed on the surface of α -Fe₂O₃ spindles using deposition-precipitation method.^[29] In deposition precipitation method, the precursor of gold is adsorbed on the surface of α -Fe₂O₃ and then reduced to obtain small nanoparticles of gold.^[29] At first gold precursors (HAuCl₄) were adsorbed on the surface of the spindles at pH 9 followed by in situ reduction, under mild conditions, 0.1 M NaOH at 70 °C to form nanoparticles of gold. NaOH was used for both purposes i.e. to maintain the basic pH at 9 and to reduce the gold precursor. At this basic pH, chloroauric acid (HAuCl₄) exists as negatively charged species [Au(OH)₄]⁻ in equilibrium with a neutral [Au(OH)₃.H₂O] species (Scheme 2a and 2b). The neutral species getting adsorbed on the negative α -Fe₂O₃ surface (Scheme 2b). Also, due to the fact that both spindle surface and a significant portion of gold precursor are negatively charged, less amount of the gold precursor was adsorbed on the spindle surface because of the electrostatic repulsion. This helps in the formation of the smaller size gold particles.



Scheme 2: (a) Relative equilibrium concentration of gold complexes as a function of pH in the solution and (b) Adsorption of Au(OH)₃ on negatively charged surface and subsequent reactions (Ref 29- reprinted with permission).

The transmission electron microscope (TEM) image of gold nanoparticles formed on the surface of spindles is shown in the Figure 4a. The gold nanoparticles are uniformly distributed over the surface of the spindles. The size distribution histogram in Figure 4b shows narrow particle size distribution with average diameter of 2.6 nm. Also, it should be noted that all the particles were less than 5 nm in size, which is the size regime of gold nanoparticles to be active for the CO oxidation.^[1, 10]

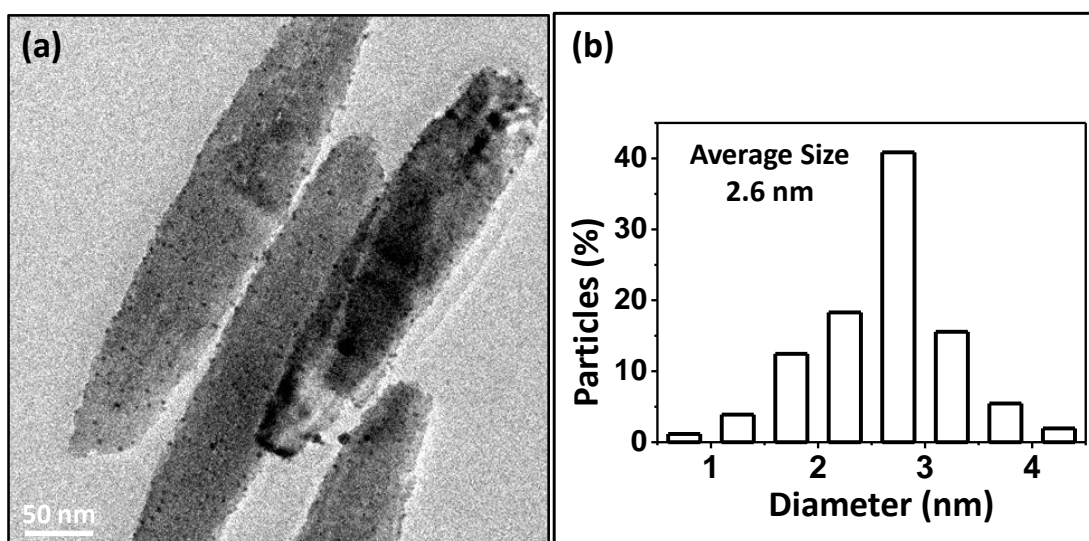


Figure 4: (a) TEM image of gold nanoparticles (2 mM HAuCl₄) deposited on the surface of α -Fe₂O₃ spindles. (b) Histogram of size distribution of the particles (counted over 250 particles).

We also studied the effect of concentration of gold precursor on the nanoparticle size and distribution. For 5 mM concentration of HAuCl₄ (Figure 5a), average diameter of gold nanoparticles is around 2.8 nm. The average particle size increases to 3.7 nm in the case of 10 mM concentration of HAuCl₄ (Figure 5b) with increase in density of particles. The increase in particle size is due to more amount of gold precursor adsorption on α -Fe₂O₃ surface which grows into larger particles in the reduction process.

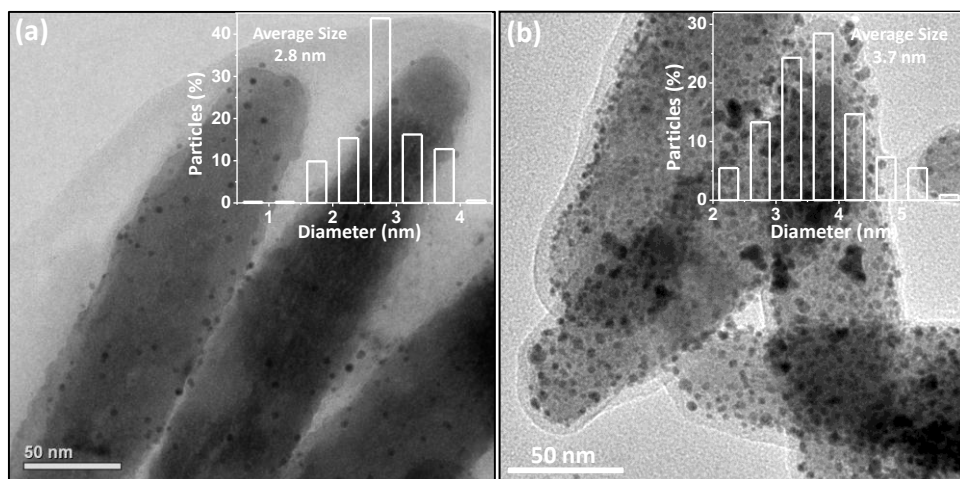


Figure 5: TEM images of gold nanoparticles deposited on the surface of α - Fe_2O_3 spindles at different precursor concentration (a) 5 mM HAuCl_4 and (b) 10 mM HAuCl_4 . Inset shows the histogram of size distribution of the particles (counted over 250 particles).

The gold precursor, HAuCl_4 was adsorbed at pH 9 maintained by the addition 0.1 M NaOH solution and then reduced at 70 $^\circ\text{C}$ in basic condition. Figure 6 shows the

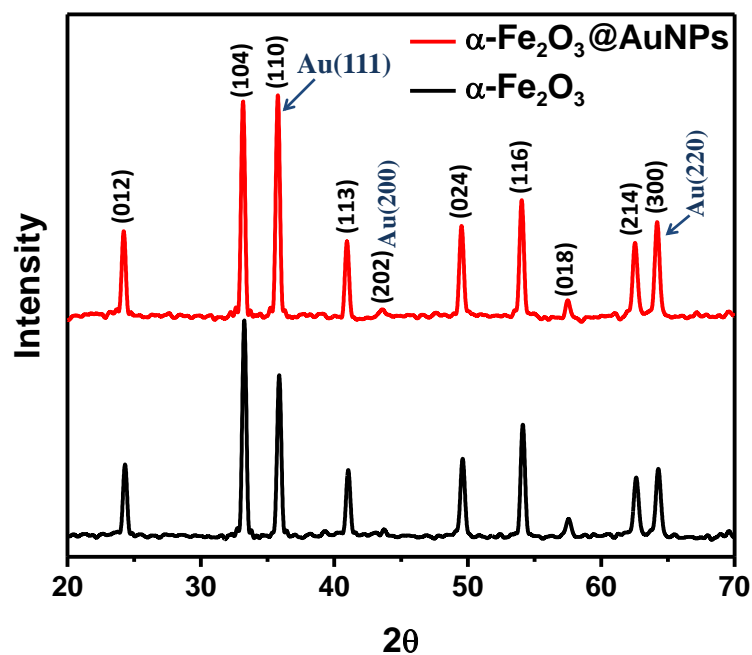


Figure 6: Powder XRD pattern of α - Fe_2O_3 @AuNPs and α - Fe_2O_3 .

powder XRD pattern of the composite having, gold nanoparticles (for 2 mM concentration of HAuCl_4) attached on the surface of the $\alpha\text{-Fe}_2\text{O}_3$ ($\alpha\text{-Fe}_2\text{O}_3\text{@AuNPs}$). The peaks at 2θ values of 36° , 44° , and 65° were common for both iron oxide and the gold nanoparticles. These peaks corresponds to (111), (200), and (220) planes of AuNP and also to (110), (202), and (300) planes of hematite respectively.

To study the surface plasmon effect of gold nanoparticles attached on the surface of hematite spindles, UV-visible spectroscopy was done for their water dispersions. Red color $\alpha\text{-Fe}_2\text{O}_3$ particles itself show a strong absorption near 430 nm and a weak absorption near 530 nm (Figure 7) due to charge transfer from 2p-orbital of oxygen to partially filled d-orbitals of iron. The UV-visible spectrum for $\alpha\text{-Fe}_2\text{O}_3\text{@AuNPs}$ was similar to that of the $\alpha\text{-Fe}_2\text{O}_3$ (Figure 7). It could happen due to two reasons: i) the surface plasmon band of the gold nanoparticles also appears in this region and is apparently

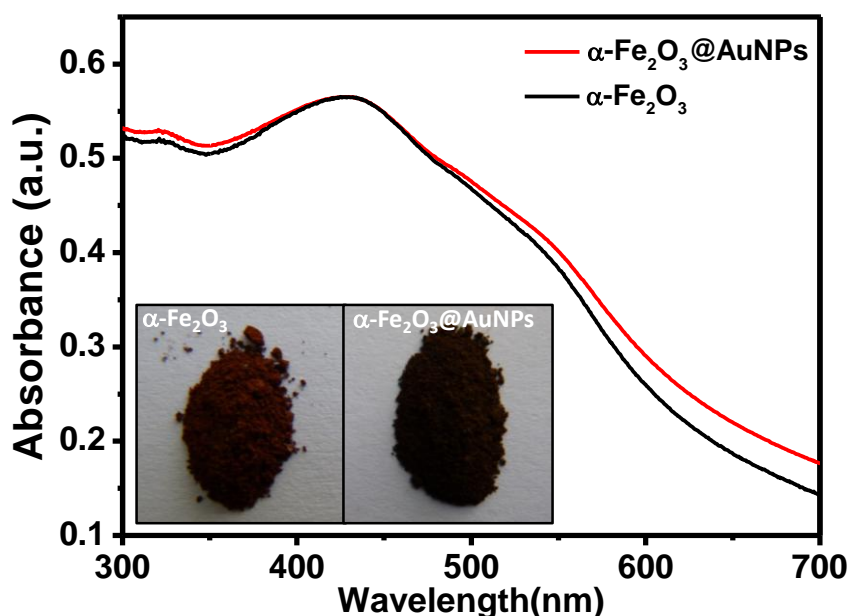


Figure 7: UV-visible Spectra of $\alpha\text{-Fe}_2\text{O}_3$ and $\alpha\text{-Fe}_2\text{O}_3\text{@AuNPs}$. Inset images show the colour of those two.

merged with the charge transfer bands of the α -Fe₂O₃ which is the major component of the composite or ii) very small gold nanoparticles (\sim 2.5 nm) does not show any surface plasmon band. Though the two samples were similar with respect to their absorption, their colors appear to be different (inset of Figure 7). α -Fe₂O₃@AuNPs was darker as compared to α -Fe₂O₃.

As the reduction conditions were mild only heterogeneous nucleation took place forming gold nanoparticles on the surface of the spindles. It was evident from the UV-visible spectra (Figure 8a) of the supernatant collected after 1 h of reduction. Also, the color of the supernatant is similar to the color of HAuCl₄ solution and this visually indicates that there were no gold nanoparticles in the supernatant (Figure 8a inset). When this supernatant was reduced using sodium borohydride it turned colored and its UV-visible spectra presented a strong absorption at 525 nm, indicating the formation of gold nanoparticles (Figure 8b). This means that not all the gold precursor got reduced in the mild NaOH reduction (at 70 °C) within 1h.

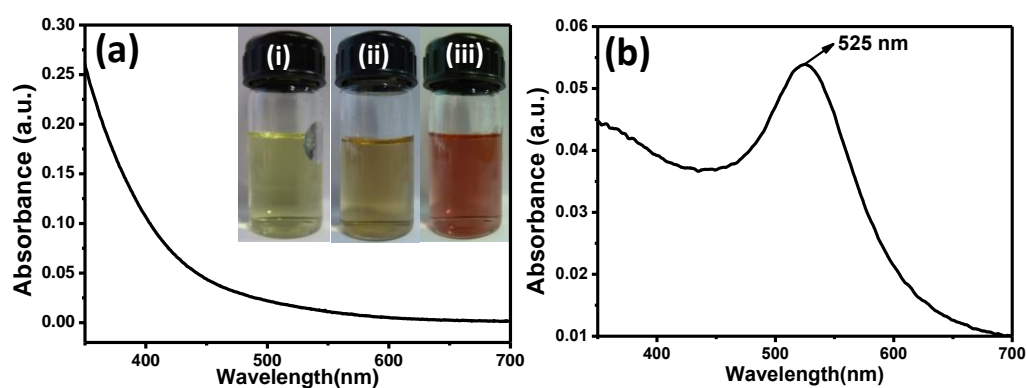
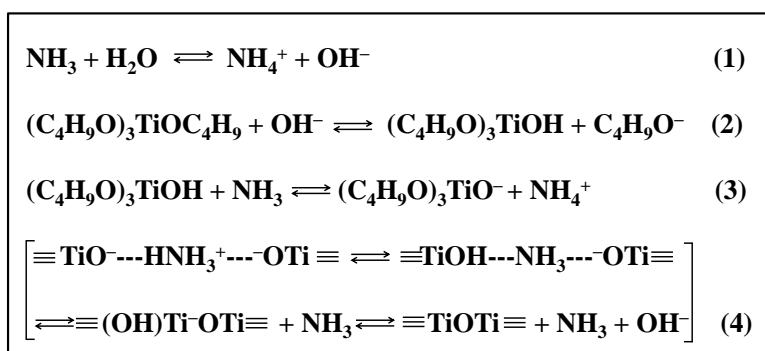


Figure 8: (a). UV-visible spectra of the supernatant, collected by centrifuging the reduction mixture. (b) UV-visible spectra of the supernatant after reduction with NaBH₄. Inset of (a) shows color of (i) HAuCl₄, (ii) supernatant, and (iii) supernatant after reduction with NaBH₄.

Following the formation of gold nanoparticles on the surface of the spindles we carried out titania (TiO₂) coating. Initially, to standardize the method we coated titania over bare α -Fe₂O₃ surface. Titania coating was done using sol-gel method. The sol-gel method is based on the inorganic polymerization reactions. Precursors of metal or non-metal alkoxides hydrolyze to alcohol followed by condensation in presences of acid or base as catalysts.^[57] In the case of titania (TiO₂) synthesis, method consists of two steps: i) hydrolysis of the titania precursor, tetrabutoxide orthotitanate (TBOT) followed by ii) condensation of the hydrolyzed products in presence of ammonia.^[55, 56] In this method, ammonium ions (NH₄⁺) play a crucial role as catalyst in the both, hydrolysis as well as condensation reactions of TBOT (Scheme 3).^[58] Apart from this, during the coating process, the positively charged ammonium ions are adsorbed first on the surface of α -Fe₂O₃ which attract negatively charged $\equiv\text{TiO}^-$ species (intermediate hydrolyzed products) and make the condensation reaction to occur on the surface.^[55]



Scheme 3: Hydrolysis and condensation mechanism of TBOT in the presence of ammonia.

We chose to work with 3:1 ethanol-acetonitrile solvent mixture for coating titania on the spindles, which plays an important role in this particular surface coating reaction. This effect of volume ratios of mixed solvents on the formation of titania coatings can be explained by the diffusion rate of TBOT and its hydrolysate onto the surface in mixed

solvent.^[58] In the presence of ammonia, the hydrolysis of TBOT molecules leads to the formation of the hydrolysates (semi hydrolyzed products) of TBOT that coexist with TBOT in the solution. The TBOT molecules and their hydrolysates have a high solubility in ethanol indicating the relatively strong interaction between the solute and the solvent molecules whereas, in acetonitrile it is just the reverse. As a result, when a certain amount of acetonitrile is added to ethanol containing TBOT solution, the interaction between the solute of TBOT and their hydrolysate molecules with the mixed solvents will be weakened. Therefore, TBOT and their hydrolysates in the mixed solvent can easily diffuse onto the surface and then hydrolyze and condense to form a titania coating.

The surface charge (zeta potential) of hematite spindles measured in the ethanol-acetonitrile (3:1) solvent is $+12.0 \pm 0.2$ mV. If positively charged NH_4^+ ions to get adsorbed on $\alpha\text{-Fe}_2\text{O}_3$ surface, the surface need to be negatively charged. Therefore, the surface of the spindles was treated with 0.1 M citric acid (CA) solution to render it

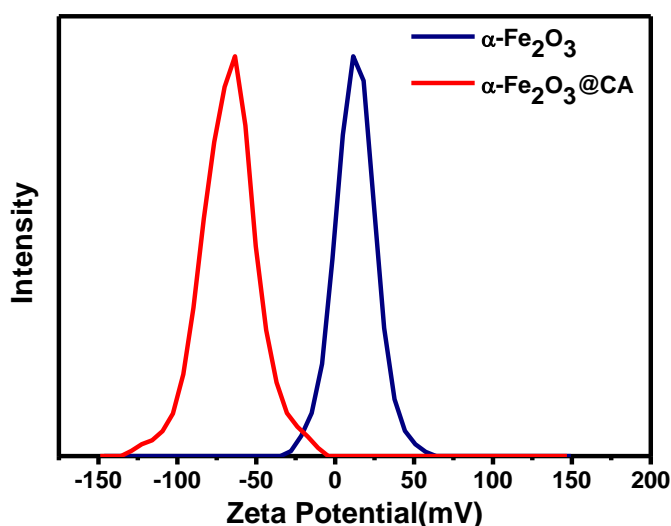


Figure 9: Zeta potential distribution of $\alpha\text{-Fe}_2\text{O}_3$ and $\alpha\text{-Fe}_2\text{O}_3\text{@CA}$.

negatively charged (Zeta Potential – 67.0 ± 0.8 mV). Figure 9 shows the zeta potential distribution of α -Fe₂O₃ and α -Fe₂O₃@CA in the mixed solvent.

We started titania coating using the reported procedure^[55] and optimized it for spindles by varying the volume of the titania precursor keeping the other factors constant (Table 1). The starting reaction was carried out using 0.3 mL of TBOT and 0.5 mL of ammonia solution in 60 mL mixed solvent (ethanol : acetonitrile, 3:1) for 1.5 h. In this case, particles are almost not coated confirmed by measuring the width of the spindles from the FESEM images (Figure 10) which is comparable with the bare spindles.

Table 1: Titania coating using different volume of TBOT:

Sample No.	Vol. of NH₃ (mL)	Reaction time (h)	Vol. of TBOT (mL)	Average width of the spindle at middle (nm)
1	0.5	1.5	0.3	85
2	0.5	1.5	0.5	100
3	0.5	1.5	0.75	165
4	0.5	1.5	0.6	160

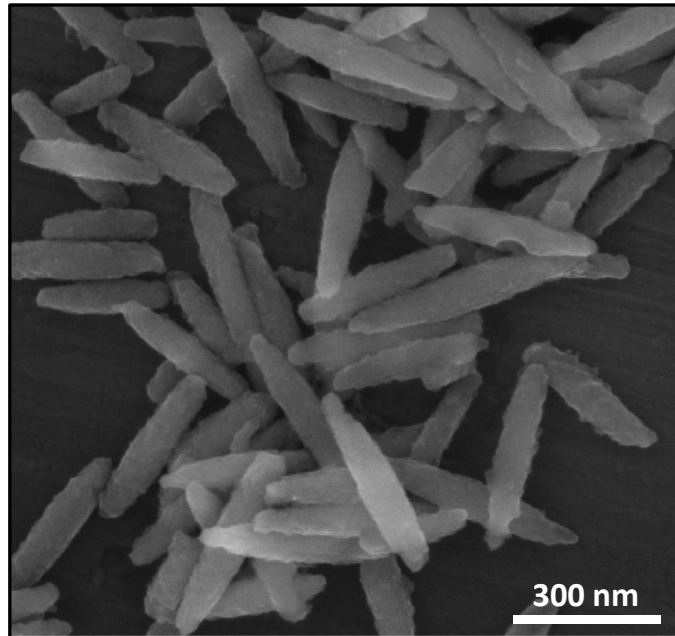


Figure 10: FESEM image of $\alpha\text{-Fe}_2\text{O}_3\text{@TiO}_2$ (vol. of NH_3 , 0.5 mL and vol. of TBOT, 0.3 mL).

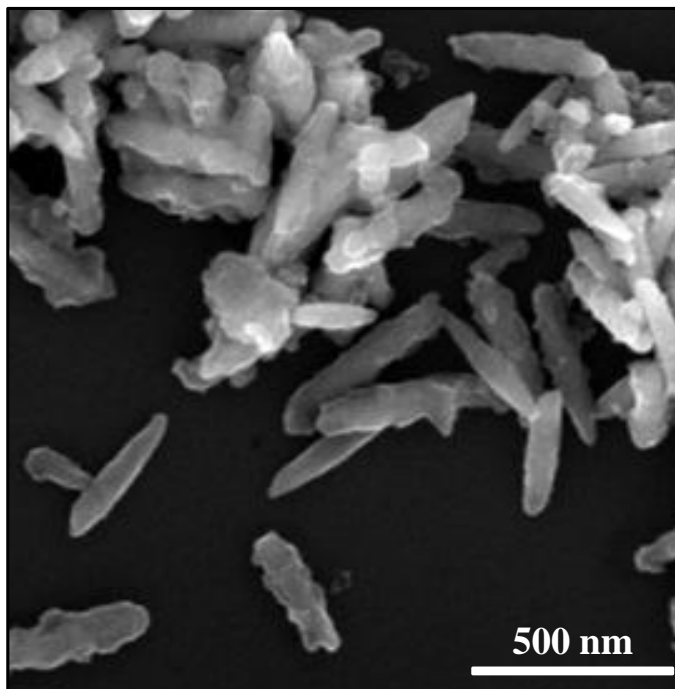


Figure 11: FESEM image of $\alpha\text{-Fe}_2\text{O}_3\text{@TiO}_2$ (vol. of NH_3 , 0.5 mL and vol. of TBOT, 0.5 mL).

Then the volume of TBOT was increased to 0.5 mL keeping all other parameter constant. In this case, coating appeared to be very uneven and non-uniform. As FESEM image in Figure 11 shows many of the particles are not even coated.

Further, increasing of the volume of TBOT to 0.75 mL in same conditions, the coating was significantly improved and the average thickness is around 40 nm shown in the FESEM image (Figure 12). But overall the sample is not cleaned and some extra particles are formed which could not be removed by washing.

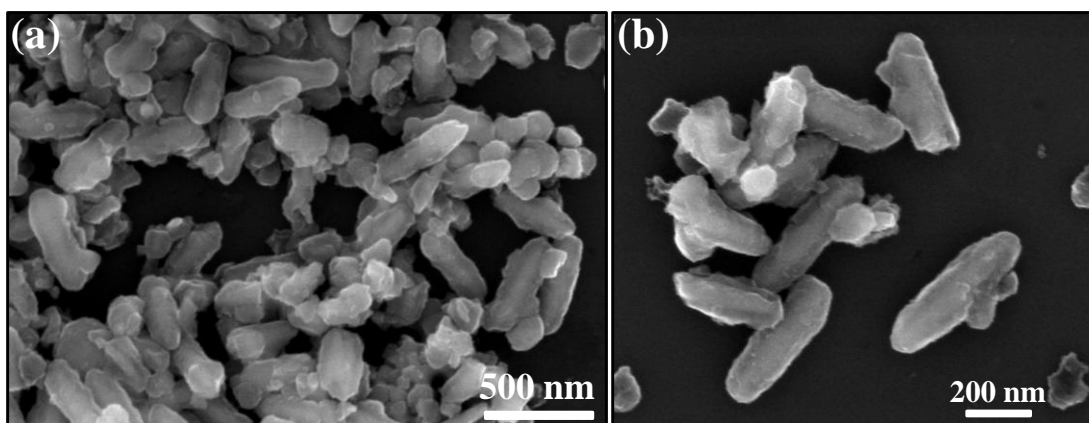


Figure 12: FESEM image of (a) $\alpha\text{-Fe}_2\text{O}_3\text{@TiO}_2$. (b) Higher magnification image of the same (vol. of NH_3 , 0.5 mL and vol. of TBOT, 0.75 mL).

In order to get the cleaned sample with uniform coating thickness the volume of TBOT was slightly reduced to 0.6 mL in same condition. Where the thickness of titania coating is remained almost same like previous sample (Figure 13). Table 1 lists the average thickness of titania coating varying the volume of TBOT keeping all other conditions same.

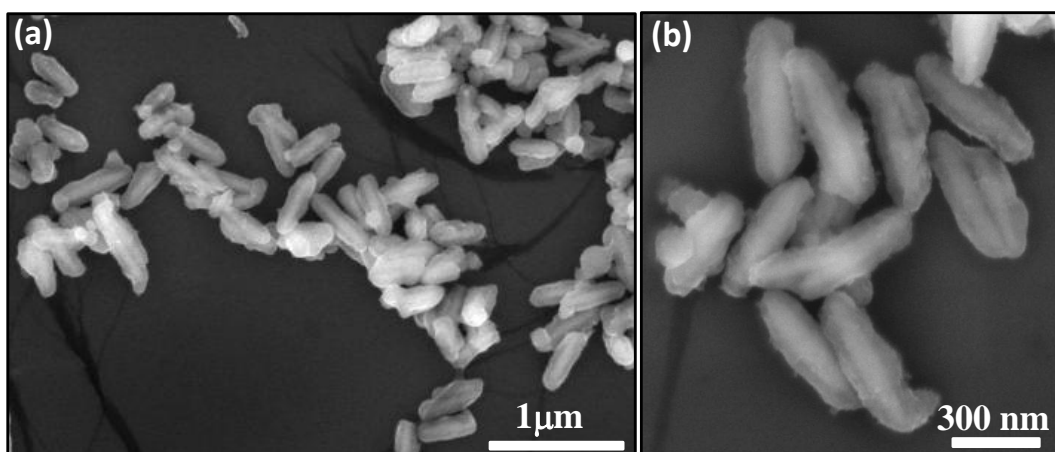


Figure 13: (a) FESEM image of $\alpha\text{-Fe}_2\text{O}_3\text{@TiO}_2$. (b) Higher magnification image of the same. (vol. of NH_3 , 0.5 mL and vol. of TBOT, 0.6 mL).

Among the above three reactions last one was the best where volume of TBOT was 0.6 mL and individual TiO_2 coated $\alpha\text{-Fe}_2\text{O}_3$ spindles were obtained with uniform thickness of titania. To adopt the same procedure to coat $\alpha\text{-Fe}_2\text{O}_3\text{@AuNPs}$ with TiO_2 , first surface charge was measured in the mixed solvent and it showed similar charge like

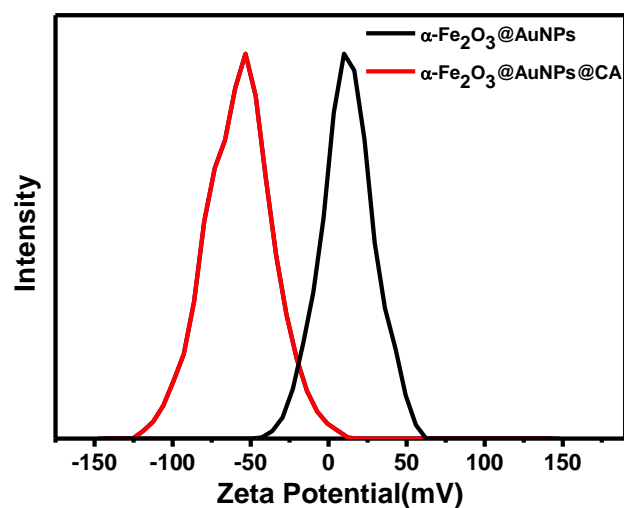


Figure 14: Zeta potential distribution of $\alpha\text{-Fe}_2\text{O}_3\text{@AuNPs}$ and $\alpha\text{-Fe}_2\text{O}_3\text{@AuNPs@CA}$.

$\alpha\text{-Fe}_2\text{O}_3$ ($+12\pm 0.2$ mV). When its surface was functionalized with 0.1 M citric acid solution, the surface charge became -56 ± 0.8 mV as expected. Figure 14 shows the zeta potential distribution of $\alpha\text{-Fe}_2\text{O}_3\text{@AuNPs}$ and $\alpha\text{-Fe}_2\text{O}_3\text{@AuNPs@CA}$ in the mixed solvent after functionalization with citric acid.

Before starting the titania coating over CA adsorbed $\alpha\text{-Fe}_2\text{O}_3\text{@AuNPs}$, the size of the gold nanoparticles were measured (Figure 15). The histogram shows broad size distribution (inset of Figure 15) with an average size around 14.8 nm (counted over 150 particles) which is larger compared to its initial size (2.6 nm) before CA treatment.

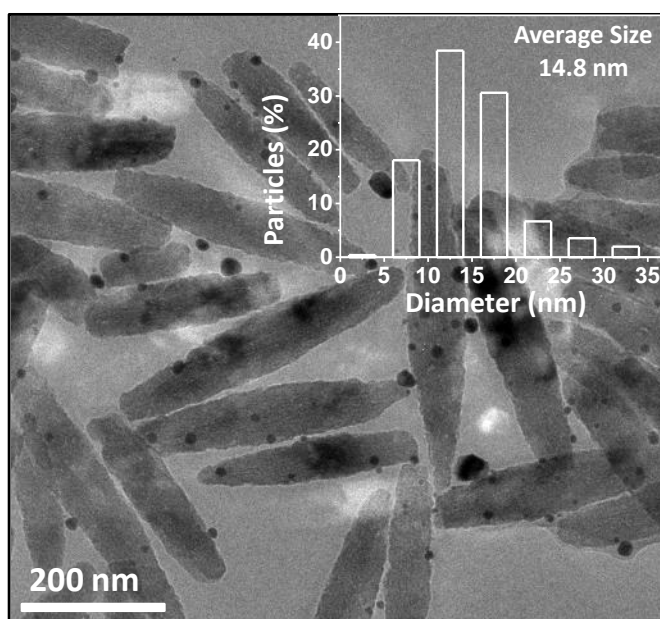


Figure 15: TEM image of $\alpha\text{-Fe}_2\text{O}_3\text{@AuNPs}$ after citric acid functionalization. Inset shows the histogram of size distribution of the particles (counted over 150 particles).

So, as a next step we replaced citric acid with a polyanion polystyrene sulfonate (PSS) in order to render the negative surface charge to the iron oxide surface in the mixed solvent. As expected, surface charge of $\alpha\text{-Fe}_2\text{O}_3\text{@AuNPs}$ became negative (-59 ± 0.8 mV)

after PSS coating (Figure 16). But the size of the gold nanoparticles were again increased (Figure 17). The average nanoparticles size is around 5.3 nm and most of the particles were having size greater than 5 nm (inset of Figure 17).

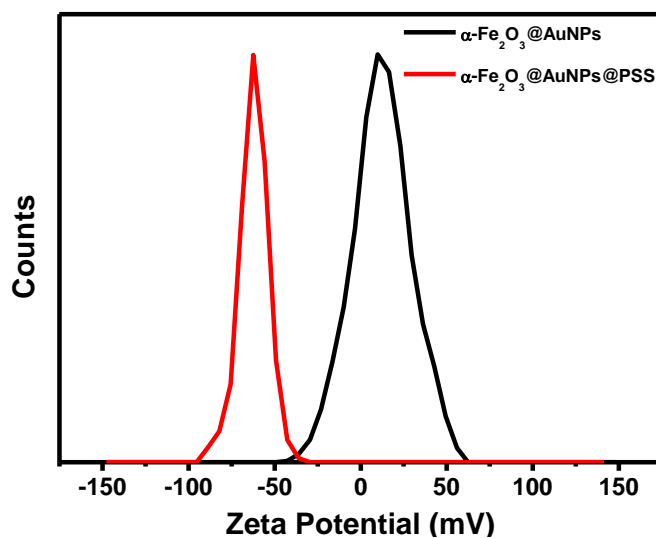


Figure 16: Zeta potential distribution of $\alpha\text{-Fe}_2\text{O}_3\text{@AuNPs}$ and $\alpha\text{-Fe}_2\text{O}_3\text{@AuNPs@PSS}$.

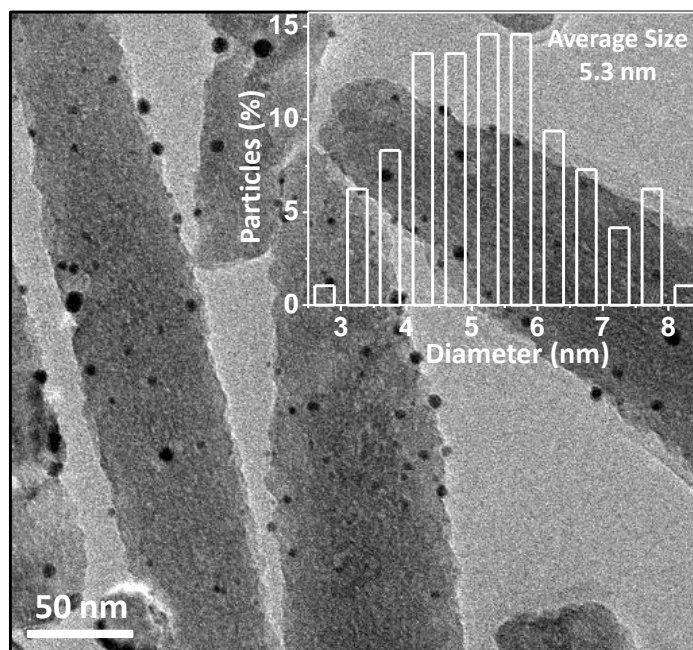


Figure 17: TEM image of $\alpha\text{-Fe}_2\text{O}_3\text{@AuNPs}$ after coating with PSS. Inset shows the histogram of size distribution of the particles (counted over 150 particles).

Then we looked into the influence of solvent mixture (used for TiO₂ coating) on the gold nanoparticle growth. When α -Fe₂O₃@AuNPs (with average particle size of gold 2.6 nm) samples were soaked in ethanol-acetonitrile (3:1) solvent mixture for 2 h, the average gold particles size increased to 5.4 nm (Figure 18). This clearly indicates that the mixed solvent aids the particle growth probably due to change in the nature of polarity of the solvent compared to water alone.

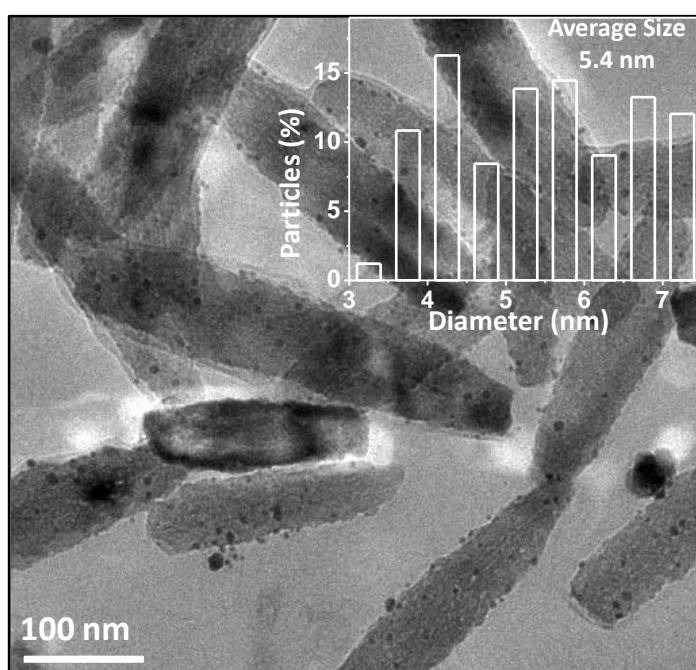


Figure 18: TEM image of α -Fe₂O₃@AuNPs after 2 h soaking in ethanol-acetonitrile (3:1) mixed solvent. Inset shows the histogram of size distribution of the particles (counted over 150 particles).

However, we found that the particle size remains unaltered and stable when α -Fe₂O₃@AuNPs soaked in ethanol (Figure 19). The average particle size is around 2.8 nm calculated from the histogram (inset of Figure 19) which is almost similar to initial size.

As evidence in the TEM image, particle density per spindles remains same and all the particles having the size less than 5 nm.

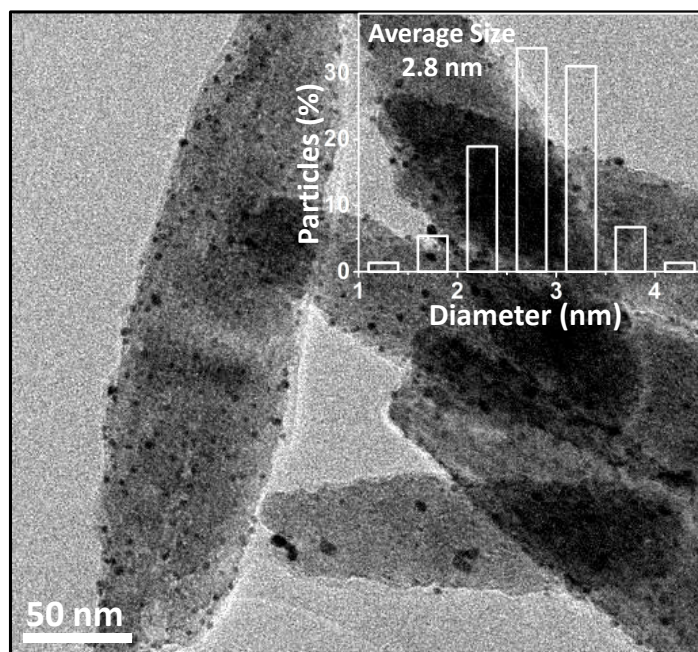


Figure 19: TEM image of $\alpha\text{-Fe}_2\text{O}_3$ @AuNPs after 12 h soaking in ethanol. Inset shows the histogram of size distribution of the particles (counted over 150 particles).

The titania coating reaction was carried out at 45 °C in ethanol in the presence of ammonia by kinetically controlled process.^[56] The titania coating reaction was done over iron oxide spindle first with varying the volume of TBOT to get desired thickness. The reaction was carried out with 0.2 mL TBOT and 0.2 mL of ammonia at 45 °C for 12 h. The FESEM image (Figure 20) shows that the spindles are almost non-coated as confirmed by measuring the width of the spindles before and after TiO_2 coating.

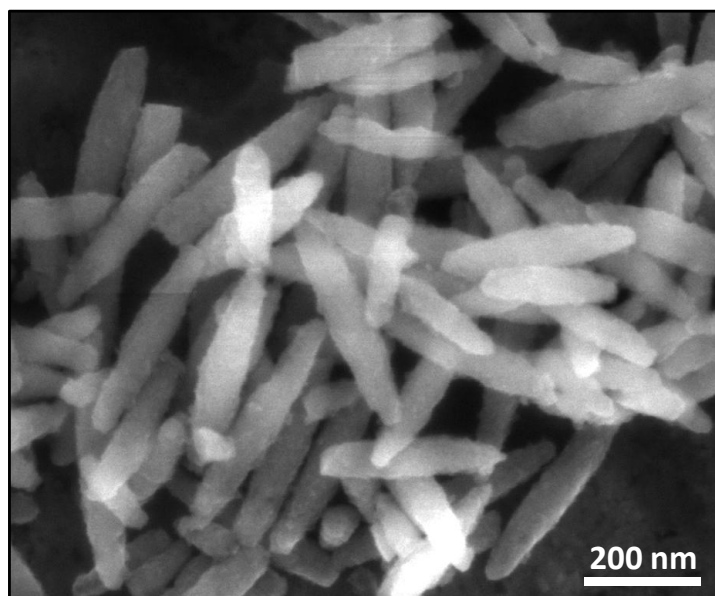


Figure 20: FESEM image of $\alpha\text{-Fe}_2\text{O}_3\text{@TiO}_2$ (vol. of NH_3 , 0.2 mL and vol. of TBOT, 0.2 mL).

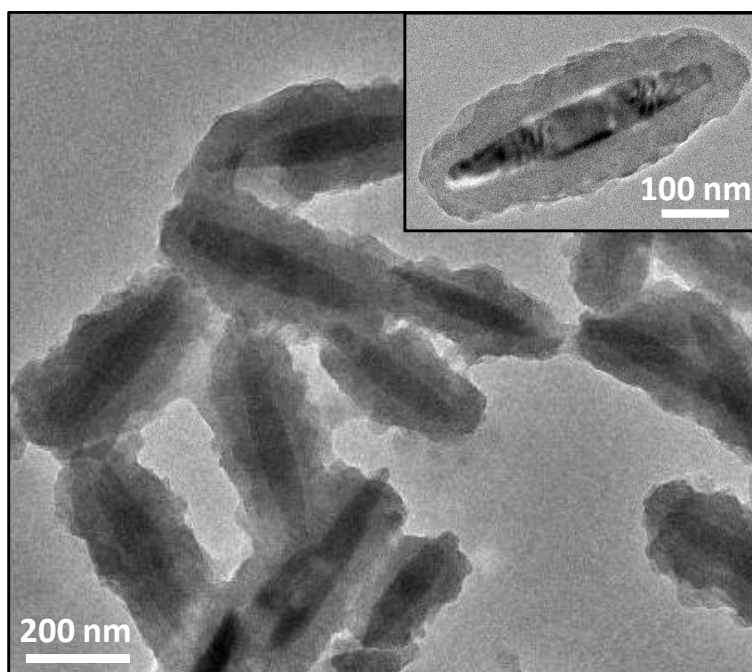


Figure 21: TEM images of $\alpha\text{-Fe}_2\text{O}_3\text{@TiO}_2$. Inset shows the thickness around 60 nm. (vol. of NH_3 , 0.2 mL and vol. of TBOT, 0.5 mL).

In the next reaction the volume of TBOT was increased to 0.5 mL keeping all other conditions constant. In this case, titania coating was observed from the TEM images (Figure 21) with uniform thickness around 60 nm and the spindles are almost separated.

Powder XRD (Figure 22) was done to know the nature of titania layer over α - Fe_2O_3 spindles. The absence of crystalline peaks observed for TiO_2 supports the formation of amorphous titania layer.

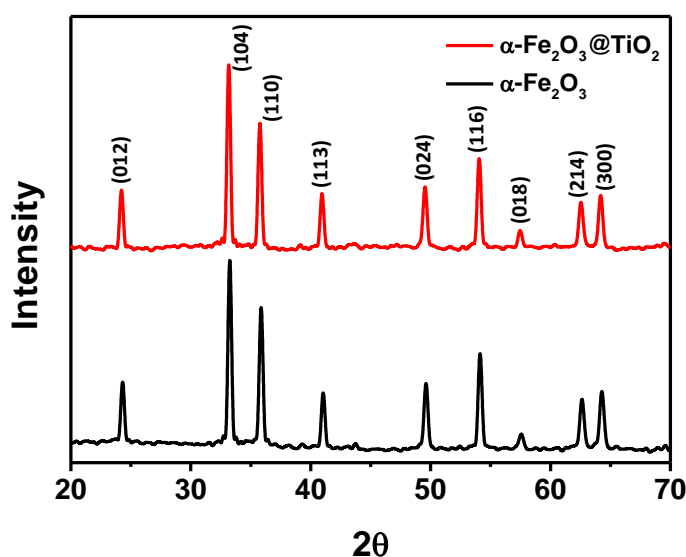


Figure 22: Powder XRD pattern of α - Fe_2O_3 and α - Fe_2O_3 @ TiO_2 .

The above experiment for titania coating was done for α - Fe_2O_3 @AuNPs taking 0.2 mL ammonia and 0.5 mL of TBOT for 12 h at 45 °C. In this case the thickness of the titania is very less (Figure 23 a) and it is showing almost no coating (23 b). The average size of the gold nanoparticles is around 3.3 nm which corresponds that there no significant change in the size during the reaction. From the histogram (23 c), it is clear that all the particles are also having size less than 5 nm.

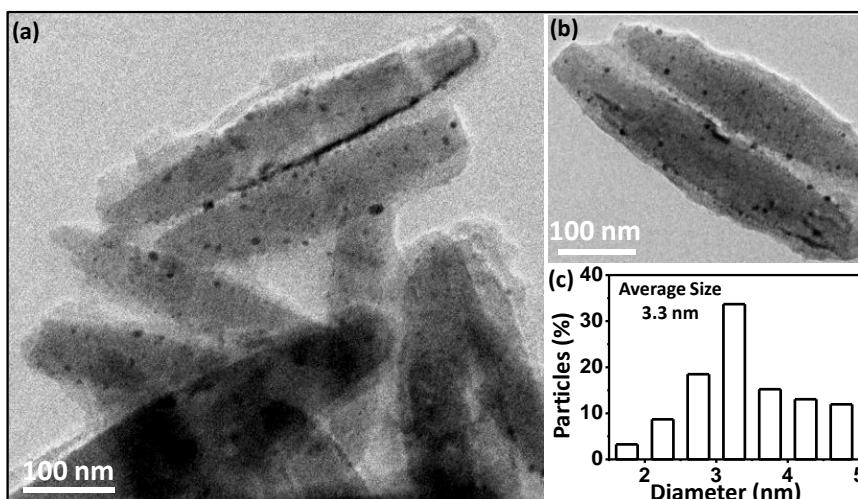


Figure 23: TEM images of $\alpha\text{-Fe}_2\text{O}_3\text{@Au@TiO}_2$ with (a) less coating and (b) almost no coating (vol. of NH_3 , 0.2 mL and vol. of TBOT, 0.5 mL) and (c) Histogram of size distribution of the particles (counted over 150 particles).

3.6 Conclusion:

Hematite ($\alpha\text{-Fe}_2\text{O}_3$) spindles with uniform size and distribution were prepared by hydrothermal treatment. The gold nanoparticles with a narrow size distribution were synthesized on the surface of the spindles. TEM images shows the gold nanoparticles having uniform size and distribution over the spindles. The size of the gold nanoparticles increases in presence of citric acid, PSS and in ethanol-acetonitrile solvent mixture where the size remains constant in ethanol solvent. The titania coating carried out by hydrolysis and condensation of TBOT on $\alpha\text{-Fe}_2\text{O}_3$ spindles in ethanol solvent. Optimization of titania coating over $\alpha\text{-Fe}_2\text{O}_3\text{@AuNPs}$ and subsequent conversion of amorphous titania shell to mesoporous crystalline, anatase TiO_2 will be carried out in future studies. Furthermore the application of these core-shell nanoparticle, $\alpha\text{-Fe}_2\text{O}_3\text{@AuNPs@mTiO}_2$ for low-temperature and high-temperature oxidation of CO will also be carried out.

3.7. References:

- [1] M. Haruta, T. Kobayashi, H. Sano, N. Yamada, *Chem. Lett.* **1987**, *16*, 405.
- [2] A. Y. M. Jones, P. K. W. Lam, *Sci. Total Environ.* **2006**, *354*, 150.
- [3] J. A. Raub, V. A. Benignus, *Neuroscience and Biobehavioral Reviews* **2002**, *26*, 925.
- [4] G. Avgouropoulos, T. Ioannides, C. Papadopoulou, J. Batista, S. Hocevar, H. K. Matralis, *Catal. Today* **2002**, *75*, 157.
- [5] R. Davda, J. Dumesic, *Angew. Chem. Int. Ed.* **2003**, *42*, 4068.
- [6] P. Lopes, K. Freitas, E. Ticianelli, *Electrocatalysis* **2010**, *1*, 200.
- [7] H. F. Oetjen, V. M. Schmidt, U. Stimming, F. Trila, *J. Electrochem. Soc.* **1996**, *143*, 3838.
- [8] G. Robert, P. Michael, S. Ferdi, *Catal. Sci. Technol.* **2011**, *1*.
- [9] M. Haruta, *Chem. Record.* **2003**, *3*, 75.
- [10] M. Haruta, S. Tsubota, T. Kobayashi, H. Kageyama, M. J. Genet, B. Delmon, *J. Catal.* **1993**, *144*, 175.
- [11] A. S. K. Hashmi, J. H. Graham, *Angew. Chem. Int. Ed.* **2006**, *45*, 7896.
- [12] A. Arcadi, *Chem. Rev.* **2008**, *108*, 3266.
- [13] A. S. K. Hashmi, *Chem. Rev.* **2007**, *107*, 3180.
- [14] M. Haruta, *Catalysis Surveys from Asia* **1997**, *1*, 61.
- [15] Y. Gao, N. Shao, Y. Pei, Z. Chen, X. Zeng, *ACS Nano* **2011**, *5*, 7818.
- [16] I. N. Remediakis, N. Lopez, J. K. Nørskov, *Angew. Chem.* **2005**, *117*, 1858.
- [17] N. Lopez, T. V. W. Janssens, B. S. Clausen, Y. Xu, M. Mavrikakis, T. Bligaard, J. K. Nørskov, *J. Catal.* **2004**, *223*, 232.

- [18] A. Sanchez, S. Abbet, U. Heiz, W. D. Schneider, H. Häkkinen, R. N. Barnett, U. Landman, *J. Phys. Chem. A* **1999**, *103*, 9573.
- [19] B. Geoffrey C, T. David T, *Cat. Rev. Sci. Eng.* **1999**, *41*, 319.
- [20] M.-C. Daniel, D. Astruc, *Chem. Rev.* **2003**, *104*, 293.
- [21] C. B. Geoffrey, T. T. David, *Gold Bulletin* **2000**, *33*.
- [22] A.-S. Saleh, F. C. Albert, H. T. Stuart, J. H. Graham, *Top. Catal.* **2007**, *44*.
- [23] Q. Botao, D. Youquan, *Appl. Catal. B* **2006**, *66*, 241.
- [24] Y. Liu, C.-J. Jia, J. Yamasaki, O. Terasaki, F. Schüth, *Angew. Chem. Int. Ed.* **2010**, *49*, 5771.
- [25] S. A. C. Carabineiro, N. Bogdanchikova, P. B. Tavares, J. L. Figueiredo, *RSC Advances* **2012**, *2*, 2957.
- [26] L. Philip, F. Jonathan, E. S. Benjamin, G. Tomas, A.-S. Saleh, F. C. Albert, A. H. Andrew, J. K. Christopher, M. Michiel, A. M. Jacob, O. Arjan, E. G. Stanislaw, J. H. Graham, *J. Mater. Chem.* **2006**, *16*, 199.
- [27] M. Haruta, N. Yamada, T. Kobayashi, S. Iijima, *J. Catal.* **1989**, *115*, 301.
- [28] M. M. Schubert, S. Hackenberg, A. C. van Veen, M. Muhler, V. Plzak, R. J. Behm, *J. Catal.* **2001**, *197*, 113.
- [29] F. Moreau, G. C. Bond, A. O. Taylor, *J. Catal.* **2005**, *231*, 105.
- [30] D. Widmann, R. Behm, *Angew. Chem. Int. Ed.* **2011**, *50*, 10241.
- [31] Z. Rodolfo, R.-G. Vicente, A. Yamin, M.-R. Albino, *ACS Catal.* **2012**, *2*, 1.
- [32] T. Fujitani, I. Nakamura, *Angew. Chem. Int. Ed.* **2011**, *50*, 10144.
- [33] I. Green, W. Tang, M. Neurock, J. Yates, *Science* **2011**, *333*, 736.
- [34] D. A. H. Cunningham, T. Kobayashi, N. Kamijo, M. Haruta, *Catal. Lett.* **1994**, *25*, 257.

- [35] H. Kim, H. Lee, G. Henkelman, *J. Am. Chem. Soc.* **2012**, *134*, 1560.
- [36] D. Widmann, R. Leppelt, R. Behm, *J. Catal.* **2007**, *251*, 437.
- [37] A.-G. Veronica, C. G. Bruce, *J. Catal.* **2008**, *260*, 351.
- [38] F. Romero-Sarria, L. M., *J. Phys. Chem. C* **2007**, *111*, 14469.
- [39] Z. Zheng, K. Steven, F.-S. Maria, S. Howard, *Adv. Funct. Mater.* **2008**, *18*, 2801.
- [40] G. J. Hutchings, M. Rafiq H. Siddiqui, A. Burrows, C. J. Kiely, R. Whyman, *J. Chem. Soc., Faraday Trans.* **1997**, *93*, 187.
- [41] F. Boccuzzi, A. Chiorino, S. Tsubota, M. Haruta, *J. Phys. Chem.* **1996**, *100*, 3625.
- [42] A. D. Pandey, R. Güttel, M. Leoni, F. Schüth, C. Weidenthaler, *J. Phys. Chem. C* **2010**, *114*, 19386.
- [43] D. Tibiletti, A. A. Fonseca, R. Burch, Y. Chen, J. M. Fisher, A. Goguet, C. Hardacre, P. Hu, D. Thompsett, *J. Phys. Chem. B* **2005**, *109*, 22553.
- [44] A. Knell, P. Barnickel, A. Baiker, A. Wokaun, *J. Catal.* **1992**, *137*, 306.
- [45] G. K. Bethke, H. H. Kung, *Appl. Catal. A* **2000**, *194–195*, 43.
- [46] C. K. Costello, M. C. Kung, H. S. Oh, Y. Wang, H. H. Kung, *Appl. Catal. A* **2002**, *232*, 159.
- [47] M. Daté, M. Okumura, S. Tsubota, M. Haruta, *Angew. Chem. Int. Ed.* **2004**, *43*, 2129.
- [48] S. H. Overbury, L. Ortiz-Soto, H. Zhu, B. Lee, M. Amiridis, S. Dai, *Catal. Lett.* **2004**, *95*, 99.
- [49] N. Mammen, S. Narasimhan, S. d. Gironcoli, *J. Am. Chem. Soc.* **2011**, *133*, 2801.
- [50] M. Okumura, S. Nakamura, S. Tsubota, T. Nakamura, M. Azuma, M. Haruta, *Catal. Lett.* **1998**, *51*, 53.

- [51] Z.-Y. Yuan, V. Idakiev, A. Vantomme, T. Tabakova, T.-Z. Ren, B.-L. Su, *Catal. Today* **2008**, *131*, 203.
- [52] K. Yoon, Y. Yang, P. Lu, D. Wan, H.-C. Peng, K. Stamm Masias, P. T. Fanson, C. T. Campbell, Y. Xia, *Angew. Chem. Int. Ed.* **2012**, *51*, 9543.
- [53] G. Prieto, J. Zečević, H. Friedrich, K. P. de Jong, P. E. de Jongh, *Nat Mater* **2013**, *12*, 34.
- [54] C.-J. Jia, L.-D. Sun, Z.-G. Yan, L.-P. You, F. Luo, X.-D. Han, Y.-C. Pang, Z. Zhang, C.-H. Yan, *Angew. Chem. Int. Ed.* **2005**, *44*, 4328.
- [55] W.-F. Ma, Y. Zhang, L.-L. Li, L.-J. You, P. Zhang, Y.-T. Zhang, J.-M. Li, M. Yu, J. Guo, H.-J. Lu, C.-C. Wang, *ACS Nano* **2012**, *6*, 3179.
- [56] W. Li, J. Yang, Z. Wu, J. Wang, B. Li, S. Feng, Y. Deng, F. Zhang, D. Zhao, *J. Am. Chem. Soc.* **2012**, *134*, 11864.
- [57] C. Burda, X. Chen, R. Narayanan, M. A. El-Sayed, *Chem. Rev.* **2005**, *105*, 1025.
- [58] P. Wang, D. Chen, F.-Q. Tang, *Langmuir* **2006**, *22*, 4832.